LAPPEENRANTA UNIVERSITY OF TECHNOLOGY

Faculty of Technology

Department of Electrical Engineering

Jussi Kauppila

ELECTRIC PROPULSION SYSTEM IN A MODERN SPORTS CAR

Examiners   Professor Juha Pyrhönen

                 Sami Ruotsalainen

Supervisor   Professor Juha Pyrhönen

TIIVISTELMÄ

Lappeenrannan teknillinen yliopisto

Teknillinen tiedekunta

Sähkötekniikan koulutusohjelma

Jussi Kauppila

Sähköinen propulsiojärjestelmä modernissa urheiluautossa

Diplomityö 2010

67 sivua, 25 kuvaa, 14 taulukkoa, 2 liitettä

Tarkastajat   Professori Juha Pyrhönen

                Sami Ruotsalainen

Ohjaaja   Professori Juha Pyrhönen

Hakusanat: sähköauto, propulsiojärjestelmä, vaihtosuuntaaja, akusto, akunhallinta, x-prize, ERA, raceabout, EMC, EMI

Työssä suunniteltiin Helsingin Metropolia-ammattikorkeakoulun X-Prize-kilpailuun osallistuneen sähköauton propulsiojärjestelmä laitetasolla Cadence ORCAD-mallinnusohjelmalla.

Työssä suunniteltiin ajoneuvon propulsiojärjestelmä sekä suunniteltiin propulsiojännite-järjestelmän turvallisuustoiminnallisuus sähköturvallisuuden kannalta. Myös järjestel-män sähkömagneettista yhteensopivuutta tarkasteltiin odotettavissa olevien häiriöiden syntymekanismeja ja siirtoteitä tarkastelemalla. Laitekohtaisia tapoja vähentää häiriöi-den vaikutusta tutkittiin ja ehdotettiin toteutettavaksi. Kestomagneettitahtikoneen sovel-tuvuutta ajoneuvokäyttöön tutkittiin tarkastelemalla moottorin väännöntuottokykyä ja auton vääntömomenttitarvetta eri pyörimisnopeusalueilla. Työssä tarkasteltiin myös lyhyesti sähköautojen historiaa sekä tulevaisuudennäkymiä.

ABSTRACT

Lappeenranta University of Technology

Faculty of Technology

Department of Electrical Engineering

Jussi Kauppila

Electric propulsion system in a modern sports car

Master's Thesis 2010

67 pages, 25 figures, 14 tables, 2 appendices

In this thesis an electric propulsion system is designed on a device level using Cadence ORCAD. The vehicle belongs to the Helsinki Metropolia University of Applied Sciences and it is to compete in the Automotive X-Prize competition held in the USA.

In this thesis the electric propulsion system and related electric safety measures are designed. Also electro-magnetic compatibility and interferences present in the system are examined by examining the birth mechanisms and transmission paths of interference. Per device effects of interference and solutions to minimize them were examined and proposed. Suitability of permanent magnet synchronous machines for passenger vehicle use was examined by examining the torque production capability of the motor and the torque requirements of the vehicle. Also a short overview of history of electric vehicles is given.

ACKNOWLEDGEMENTS

Lappeenranta, June 14th, 2010

Jussi Kauppila

'Unelma vain on diplomityömme,
joka tenttimme vanhentunut.
:,: Jo ruostunut harpikko käyttämätön,
tushi pulloihin jähmennyt :,:'

TABLE OF CONTENTS

NOMENCLATURE

A	Area
C	Drag/Rolling Friction Coefficient, Capacitance
E	Energy
f	Frequency
F	Force
g	Gravitational Constant
I, i	Current
L	Inductance
l	Length
m	Mass or Modulation Index
P	Power
R	Resistance
t	Time
T	Time, Temperature, Torque
U, u	Voltage (DC/AC)
v	Velocity
X	Reactance
Z	Impedance
η	Efficiency
ρ	Conductivity or Air Density
ω	Angular Speed

UPPER AND LOWER INDICES

a	Modulation index
air	Air
batt	Battery
BW	Bandwidth
c	Switching Frequency, cold
charge	Charge
charger	Charger
cm	Common Mode
CO_2	Carbon Dioxide
cond	Conductor
conv	Converter
d	Drag
DC	Direct Current
den	Density
dm	Differential Mode
el	Electricity
ev	Electric Vehicle
f	Fall
fric	Friction
h	Hot
km	Kilometre
kWh	Kilowatthour
LL	Line To Line
loss	Loss
max	Maximum
MJ	Megajoule
out	Output
pack	143-Cell Battery Pack
ph	Phase
prod	Production
r	Rise

ref	Reference
rms	Root Mean Square
s	Sum, Stator
tot	Total
trans	Transmission
ttw	Tank To Wheels
wtw	Well To Wheels

LIST OF ABBREVIATIONS

AC	Alternating Current
DC	Direct Current
EDS	Emergency Disconnect System
EESS	Electric Energy Storage System
EM	Electromagnetic
EMC	Electromagnetic Compatibility
EMI	Electromagnetic Interference
ERA	Electric RaceAbout (used to refer to the car in this thesis)
EV	Electric Vehicle
IC	Internal Combustion
ICE	Internal Combustion Engine
IGBT	Insulated Gate Bipolar Transistor
PHEV	Plug-in Hybrid Electric Vehicle
PWM	Pulse Width Modulation
SOC	State Of Charge
SVM	Space Vector Modulation

1. INTRODUCTION

1.1 GOAL OF THIS THESIS

The aim of this thesis is to design a electric propulsion system for high-end electric sports car designed for limited mass production. The vehicle is going to take part in the Progressive Insurance Automotive X-Prize competition held in 2010 in USA.

The term "low voltage" originates from the European Union Low Voltage Directive (LVD) 2006/95/EC. Low voltage is defined as voltages between 75 and 1500 V DC or 50 and 1000 V AC. An electric car has usually a low voltage system and in addition to that a protective voltage system with 12 or 24 V operating traditional auxiliary systems of the car. In several common papers the low voltage system is referred to as a high voltage system. In this study, however, the term "electric propulsion system" or "propulsion voltage" is used to refer to the main motive force generation system and the 350 V traction battery voltage thus avoiding any complications arising from term "low voltage". In traditional cars there can exist also real high voltage apparatuses such as the 20 kV ignition system of Otto-motors or Xenon light supply systems operating in the range of several tens of kilovolts.

In the thesis four separate areas of interest related to the electric propulsion system are examined in order of appearance:

1. **Schematic**
   - Electric propulsion system is examined on device-level detail in Chapter 3. The goal was to produce a schematic level design of the electric propulsion system in accordance to the competing vehicle technical specification ver. 6.1.

2. **Safety**
   - Safety of the electric propulsion system is of utmost importance and strict technical requirements are placed on competing vehicles by the X-Prize organization. The goal was to design the safety measures related to the electric propulsion system in a way

that they meet the set criteria. Vehicle electric safety design is examined in Chapter 3.4.

3. **EMC**

- The goal of electro-magnetic compatibility (EMC) design in this thesis was to ensure continued functionality of both the propulsion voltage and protective voltage (12 V) systems. Different kinds of interference, their birth mechanisms and ways to minimize their effects and protect sensitive devices onboard are examined in Chapter 3.5

4. **Motors**

- In Chapter 4 the motors found in ERA are examined in closer detail. The goal was to examine current motors and their suitability to be used in electric vehicles.

In addition in Chapter 2 a short introduction is given to electric vehicles and how they differ on structural level from vehicles powered by internal combustion engines. Also their environmental effects are examined to provide a solid reason why the continued development of electric vehicles is of interest.

1.2 STRUCTURE OF THIS THESIS

In the second chapter electric vehicles are examined on a general level to give the reader a perspective to this work. First a short history is given, followed by examination of environmental effects of electric vehicles. Also the effect the increased electric vehicle base is going to have on the electric infrastructure is examined.

In the third chapter the electric propulsion system is first presented on a device-level schematic. In the following chapters each of the primary components are examined in their own chapters. Next a short overview of the different secondary components is given. In Chapter 3.4 the electric safety measures and their behaviour is examined. EMC and EMI, their birth mechanisms, effects on the system and ways to minimize their effects are examined in Chapter 3.5. Last part of Chapter 3 considers the efficiency and mileage of the vehicle.

In Chapter 4 the permanent magnet synchronous motors are examined in closer details. Chapter 4 also covers the examination of suitability of PMSM for vehicle use and the different torque requirements placed on the motors.

2. INTRODUCTION TO ELECTRIC VEHICLES

While gaining worldwide public interest during the latest 20 years the electric car itself is an old invention predating the first gasoline combustion engines by several decades. First self-propelled carriages were running on steam engines at the end of 18th century. Nicolas Joseph Cugnot is often regarded as the inventor of the first automobile and was the very first person to get into a motor vehicle accident in 1771 when he drove his steam-powered carriage towards a stone wall. Electric vehicles saw the daylight sometime between 1832 and 1839 when the first electrically powered carriage was invented by Scotsman Robert Anderson immediately after the invention of the magnetic induction by lector Michael Faraday in 1831 and the first primitive electric motors. Slow and cumbersome vehicles evolved quickly into sleek roadsters which were superior to their steam- and gasoline-powered counterparts. The first golden era of electric vehicles lasted well into the 20th century. The decline began in 1920s when, with the improved infrastructure, longer operating distances became important. Relatively cheap crude oil and the invention of electric starter were the first severe blows. With the advent of first cheap, effectively mass-produced gasoline-powered automobiles by Henry Ford the electric car was quickly forgotten.

Recent rise of interest in climate change saw also the rise of interest in alternative propulsion and fuel sources. Hybrid, pure electric, hydrogen, fuel cells et cetera are topic of the day all over the globe. Progressive Insurance Automotive X-PRIZE is a set of events and competitions organized by the X-PRIZE foundation to encourage and inspire research and development of new, efficient and eco-friendly vehicles. The aim is to lessen our dependency on fossil fuels and ultimately slow down the climate change. A total of 110 teams are competing for prize money of 10 million dollars divided between three distinct classes.

Electric Raceabout (ERA) vehicle is designed by a Finnish team consisting mainly of students and staff members of Metropolia University of Applied Sciences located in Helsinki. The vehicle competes in the alternative 2 class for the grand prize of 2.5 million dollars.

ERA is a two seated vehicle that is designed from the beginning to be a sleek-looking modern sports car. ERA is propelled by four reluctance-aided permanent magnet synchronous motors. Each is capable of producing over 800 Nm of torque for a limited time and has nominal torque of 250 Nm. Powered by 33 kWh lithium titanate batteries it is capable of reaching operating range of over 200 km per charge.

Designing an electric propulsion system for an electric car is a difficult task, not made any easier by tight safety regulations and lack of standardization. Especially, worrisome are EMI problems certain to emerge in a system where there are several high powered PWM inverters and electric motors located close to sensitive 12 V wiring and systems. Fast high voltage and current transients present in the inverters will cause EM radiation and conducted interference in frequencies up to tens of megahertz. Due to this a lot of attention will be given to EMC during design process to both avoid and minimize problems and to avoid having the need to do major changes to an existing design at a later time.

2.1 ELECTRIC VEHICLE CATEGORIES

Electric vehicles are divided into several categories depending on the level and method of electrification of the main drive system. Hybrid vehicles have both an ICE and an electric motor. Hybrid vehicles are divided into two categories which in turn are divided into several subcategories. These two main categories for hybrid vehicles are parallel hybrids and series hybrids.

In parallel hybrids the electric motor is used to boost the performance of main engine, which is usually a standard ICE. Parallel hybrids are divided into three subcategories which are:

1. Mild hybrids; these vehicles use electric motor to boost the ICE's performance.

2. Strong hybrids; these vehicles are capable of running solely on the electric motor but use both the ICE and electric motor when running at full power.

3. Strong PHEVs are identical in build to strong hybrids but they have increased onboard battery capacity and can be charged with onboard charger by plugging the car into an electric outlet.

Figure 2.1 shows the basic schematic for parallel hybrid vehicle power train. Grey boxes represent differential gears. Thin connecting lines represent non-mechanical power transmission; one line for combustible fuel, two for direct current and three for three-phase alternating current. Thick connecting line is mechanical power transmission.
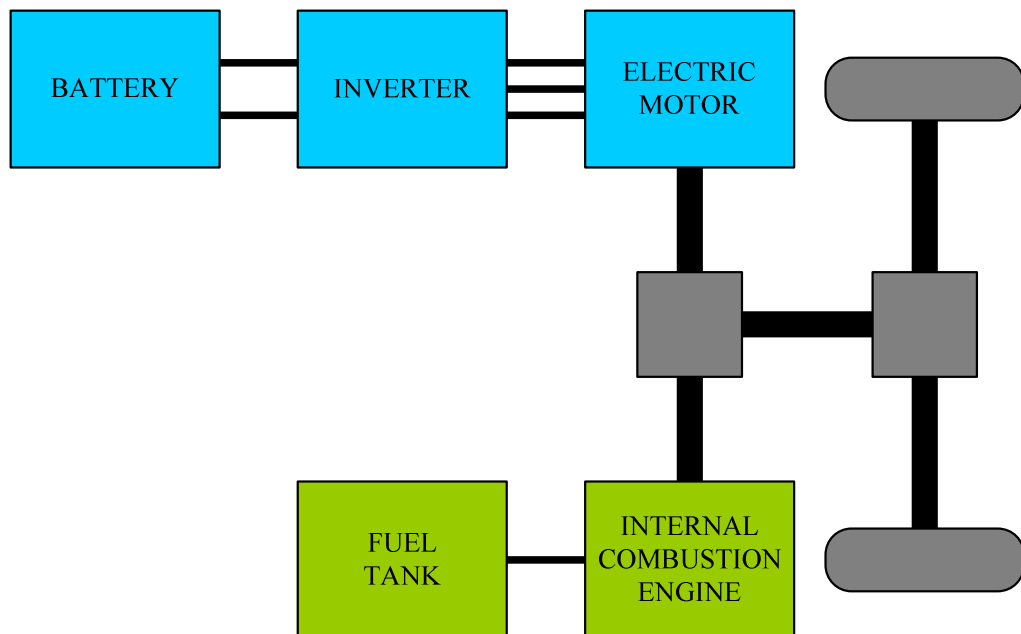
Figure 2.1 Parallel hybrid vehicle power train schematic

Series hybrids use ICE to provide power for the main electric drive system. Due to this the ICE can be used, efficiency wise, at its optimal operating point which is around 5000-6000 min^{-1}. Series hybrids are divided into two subcategories:

1. Series hybrids use ICE only to provide electric power for the electric motor, not for directly producing motive power to the wheels.

2. Series PHEVs have onboard batteries which can be charged from an electric outlet and are similar to strong parallel PHEVs.

Figure 2.2 shows the main power train schematic for a series hybrid vehicle. Depending on the configuration, the electric motor either relies solely on the battery to provide electric power or it may use both the charger and the batteries at the same time when the power need is increased due to acceleration or for other causes.
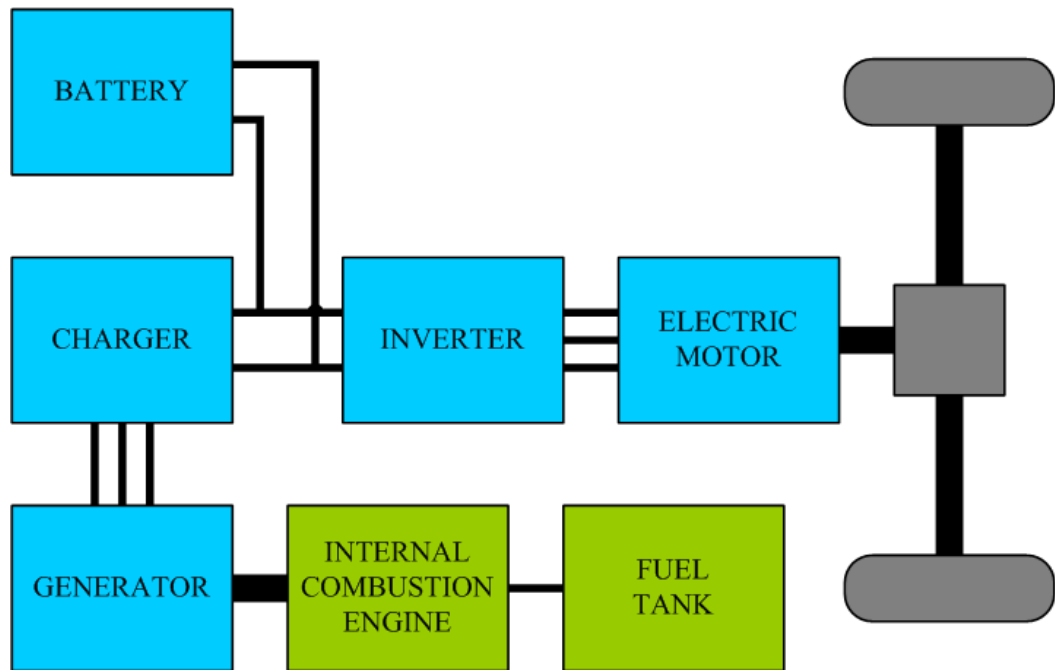
Figure 2.2 Series hybrid vehicle power train schematic

All-electric Vehicles or EVs do not use internal combustion engines at all; instead they have electric motors and sufficient onboard batteries to achieve feasible operating ranges. This eliminates the need for cumbersome ICE but the need for added battery capacity counters any advantage gained mass-wise. Usually all-electric vehicles have an internal onboard charger to allow charging the vehicle using standard electric outlets but they may also have receptacles for external high-power charging stations which allow the vehicle to be charged in minutes instead of hours. Electric motors may also be connected directly to the wheels eliminating the need for differential gears and further improving efficiency as mechanical losses that occur in gears are removed.

Figure 2.3 All-electric vehicle power train schematic

2.2 ENVIRONMENTAL EFFECTS OF ELECTRIC VEHICLES

Electric vehicles (both hybrids and fully electric vehicles) are considered to be a greener alternative for normal combustion powered ones but this is neither always the case nor is the difference as great as many believe. This misconception is due to the fact that the effects the production of electricity has on environment are not taken into consideration nor are the power transmission losses. To pr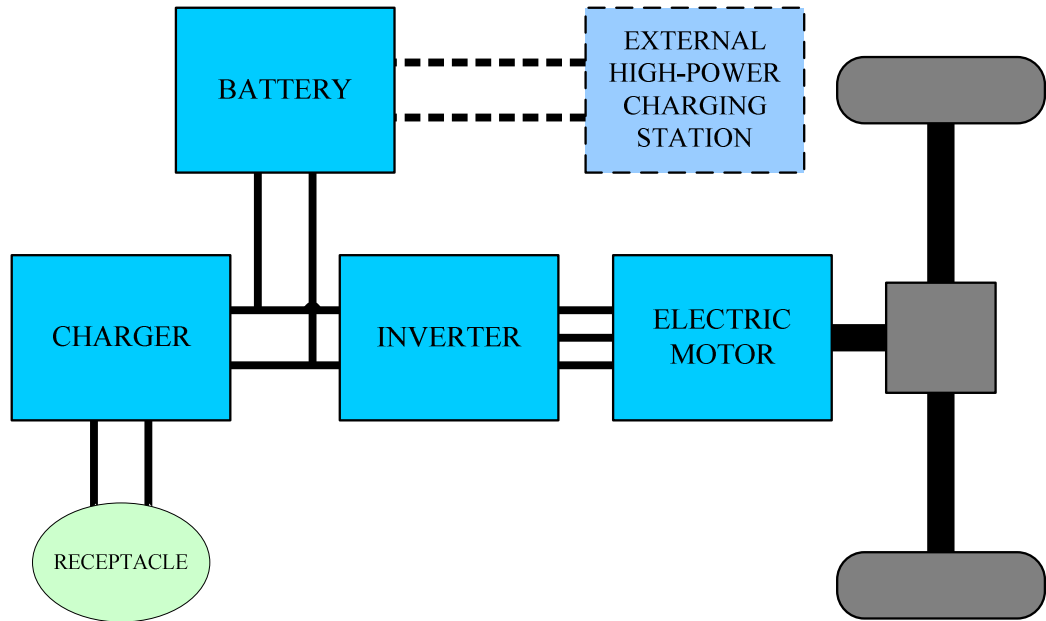operly estimate the effect, or the 'green factor', an electric vehicle has on environment we need to establish correlation factor between a unit of electric power stored in the EESS and comparable unit of fuel used in combustion engine.

Most common fuels used in combustion engines today are fossil gasoline and diesel or ethanol-based biofuels and analogues of the latter. In a petrol combustion engine the fuel-air mixture is first compressed to a higher pressure in the cylinder by a piston. Fuel is then ignited and the increased pressure created by the burning fuel pushes the piston down releasing energy stored in the fuel. In a diesel engine air is compressed alone and burning starts when high pressure hot air receives diesel fuel injection. These are the main principles by which all combustion engines work. Even though it is highly refined and well understood process it is also relatively highly inefficient when compared to the energy conversion that occurs in electric motors. Most of the energy stored in fuel is

lost as heat produced during the burning process whereas only a relatively small amount of energy obtained from volumetric expansion can be put to use. This is based on the limiting heat machine theoretical Carnot efficiency $1 - T_c/T_h$ where indices c and h refer to cold and hot temperatures of the operating cycle. As the temperatures are measured in Kelvin degrees the temperature difference in case of internal combustion engines is limited by the environment (cold) and materials (hot). In internal combustion engines the cold temperature is close to the environment temperature $\sim$ 300 K. Burning takes place in e.g. in 800 K which results in a theoretical maximum of 0.62. In practice the efficiencies are limited by several practical reasons and the efficiency of a diesel process is about 0.4 at its best. Otto process efficiency is significantly lower. While some of this thermal energy can be recovered using thermal exchangers it still remains the greatest cause for the inefficiency of internal combustion engines. Modern IC engines can reach in optimum conditions overall efficiencies of up to 30 % with 40 % peak efficiency in diesels when, in comparison, most electric motors operate at efficiencies above 85 % with permanent magnet motors reaching 96 % in the power ranges needed in passenger cars.

In Table 2.1 are given different energy and power densities for most common energy sources and EESSs. For energy sources with varying energy densities the highest known value was used. Natural gas volumetric energy density is for liquefied gas.

$$E_{\text{den,kWh}} = \frac{E_{\text{den,MJ}}}{3.6} \tag{1}$$

Specific and volumetric energy densities in kilowatt hours were calculated from known energy densities using equation (1). In equation (1) $E_{\text{den,kWh}}$ is the energy density in kilowatt hours and $E_{\text{den,MJ}}$ is energy density in megajoules.

In Table 2.1 we can see that storing electric energy in equivalent amounts to fossil and biofuels requires at least hundred times more capacity both mass- and volume wise.

Table 2.1 Comparison of energy densities of different fuels and energy storage systems /1/

Energy source	Specific energy density [MJ/kg]	Volumetric energy density [MJ/l]	Specific energy density [kWh/kg]	Volumetric energy density [kWh/l]
Fossil fuels				
Diesel	42.8	35.9	11.9	9.96
Gasoline	43.0	31.0	11.9	8.61
Natural gas	50.0	28.7	13.9	7.97
Biofuels (liquid)				
Biodiesel	37.8	35.7	10.5	9.92
Ethanol	26.8	21.2	7.4	5.89
Methanol	22.7	15.9	6.3	4.42
EESSs				
Lead-acid battery	0.108	0.100	0.030	0.028
Nickel-cadmium battery	0.288	0.240	0.080	0.067
Lithium cobalt battery	0.720	1.900	0.200	0.530
Lithium iron phosphate battery	0.400	0.792	0.110	0.220
Lithium titanate battery	0.274	0.236	0.072	0.062

If we take tank-to-wheels efficiency into account (Table 2.2 and Table 2.3) we can see that the greater energy efficiency of the electric power train helps to bridge this gap but the difference still remains great. Tank-to-wheels efficiency ratio for combustion engines was estimated to be 0.3 for diesel engines and 0.2 for gasoline engines including mechanical losses. Both are relatively high but achievable using modern engine topologies. For electric vehicles the ratio was calculated from approximated inverter efficiency of 95 %, motor efficiency of 95 % and battery discharge efficiency of 96 %.

Table 2.2 Effective energy densities in MJ /1/

Energy source	Specific energy density [MJ/kg]	Volumetric energy density [MJ/l]	"Tank-to-wheels" efficiency ratio	Effective specific energy density [MJ/kg]	Effective specific energy density[MJ/l]
Diesel	42.8	35.9	0.300	12.8	10.8
Biodiesel	37.8	35.7	0.300	8.51	8.03
Gasoline	43.0	31.0	0.200	8.60	6.20
Lithium iron phosphate battery	0.400	0.792	0.872	0.349	0.690
Lithium cobalt battery	0.720	1.900	0.891	0.642	1.693
Lithium titanate battery	0.259	0.508	0.866	0.217	0.426

From engine-efficiency correlated Table 2.2 and Table 2.2 we can see that the specific energy density gap between combustible fuels and electric energy storages is half of that without correlation.

Table 2.3 Effective energy densities in kWh /1/

Energy source	Specific energy density [kWh/kg]	Volumetric energy density [kWh/l]	"Tank-to-wheels" efficiency ratio	Effective specific energy density [kWh/kg]	Effective specific energy density[kWh/l]
Diesel	13.4	11.2	0.300	4.01	3.36
Biodiesel	10.5	9.92	0.300	3.15	2.98
Gasoline	11.9	8.61	0.200	2.39	1.72
Lithium iron phosphate battery	0.110	0.220	0.872	0.096	0.192
Lithium cobalt battery	0.200	0.528	0.891	0.178	0.470
Lithium titanate battery	0.072	0.142	0.866	0.062	0.123

From Table 2.2 and Table 2.3 we can see that one litre of gasoline is roughly equivalent of 1.7 kWh (6.2 MJ) and that we need 16 kg of lithium titanate batteries to provide the same propulsion energy for an electric motor as a litre of gasoline provides for an ICE.

Now that we have established correlation between both energy and power stored in different mediums we can compare the average consumption and consider the effects the ever-growing electric vehicle base has on power distribution and generation as well as on environment.

In Finland there are 2.7 million registered passenger cars and an average car-owner drives 18 800 kilometres annually. This translates into $51 \cdot 10^{9}$ kilometres driven annually. An average electric vehicle consumes between 0.1 and 0.3 kWh per kilometre. In Figure 2.4 is plotted the percentile of electric vehicles of the total passenger car base against the total electric energy consumed. /2/
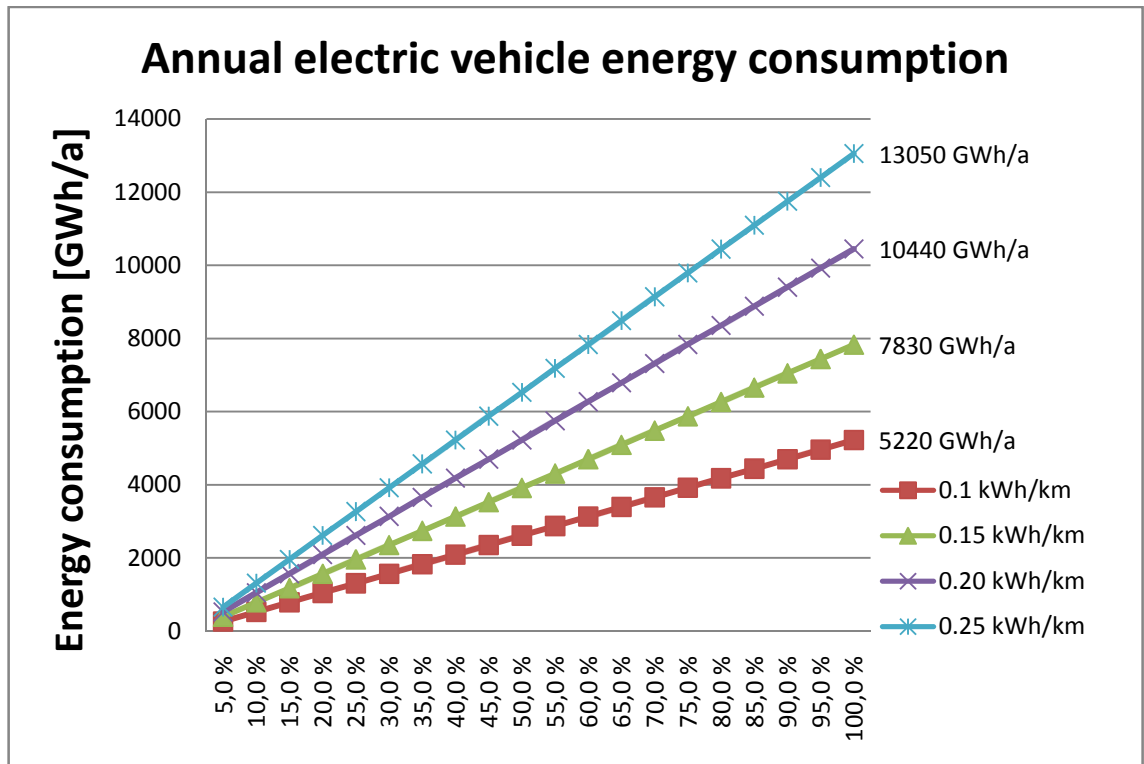

Figure 2.4 Estimated annual electric vehicle energy consumption in Finland

As can be seen in Figure 2.4, if half of the current passenger car base would be converted into electric vehicles (with estimated average consumption of 0.15 kWh/km), it would increase the annual consumption of electricity in Finland by 3900 GWh per year which is about 4 % of the Finnish annual electricity production and is roughly equal to the annual electricity production of Olkiluoto-1 nuclear reactor and 15 times the electricity produced in Finland by wind generation. /3/

To give a proper estimate of carbon-dioxide emissions from electric vehicles we need to study the present day structure of production of electricity in Finland. Most of the energy used in Finland is produced from non-renewable resources such as uranium for nuclear power and coal and oil for condensing power and cogeneration. Renewable fuel sources such as biomass, waste, hydro and wind power amount to less than one third of total energy production.

Figure 2.5 shows how the production of electricity was divided in Finland in 2007. Import of electricity was not taken into account.
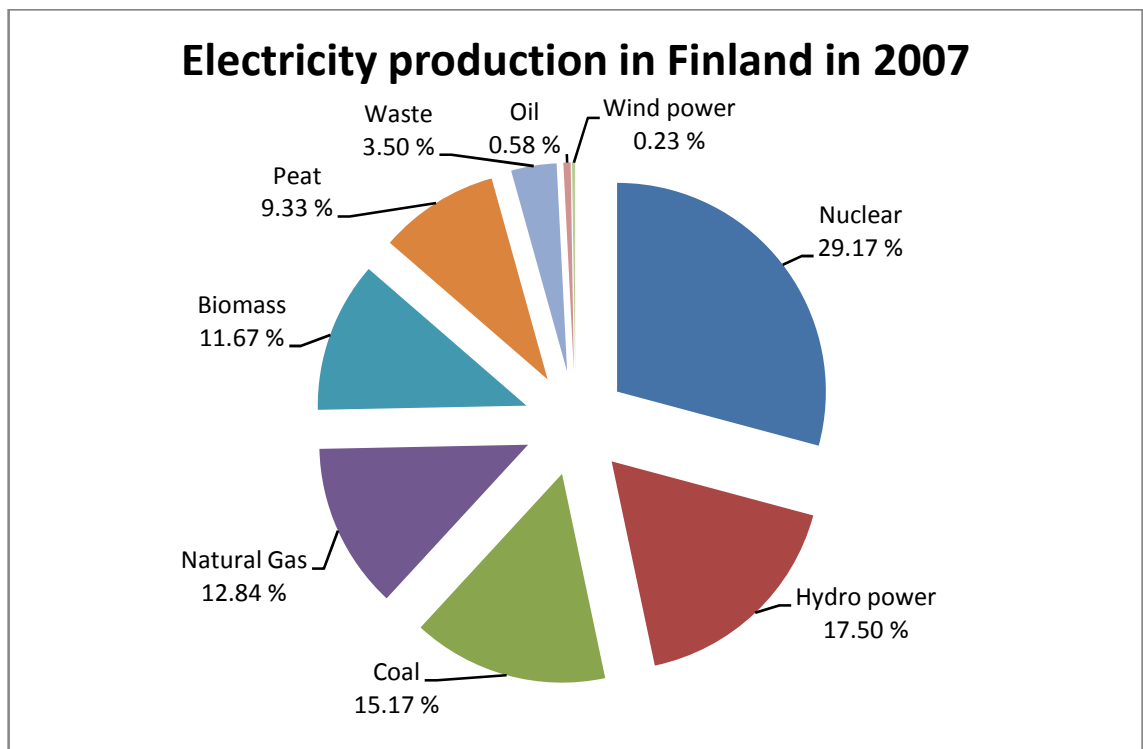

Figure 2.5 Energy production in Finland in 2007 /3/

In Table 2.6 we can see the carbon emissions for different energy sources and an estimate for total CO_2 produced per kWh of energy produced. Imported electricity is not taken into account for calculating the total production of CO_2. Carbon footprint for condensing energy generation using waste was estimated to be roughly equal to the carbon footprint of biomass. For cogeneration using oil and renewable fuel sources the total carbon emissions were multiplied with 0.4 to take into account the generation of usable heat as a byproduct of generation of electricity (*). /4/

Table 2.4 Adjusted carbon footprint, (*) denotes adjusted number /1/

Energy source	Carbon emissions CO_2 [g/kWh]	Percentage of electricity production [%]	Adjusted carbon emissions CO_2 [g/kWh]
Coal	940	15.17 %	143
Oil	260*	0.58 %	1.51
Natural gas	200*	12.84 %	25.7
Wind	23	0.23 %	0.05
Hydro	5	17.50 %	0.88
Nuclear	5	29.17 %	0.58
Biomass	32*	11.67 %	3.73
Peat	320*	8.48 %	27.1
Waste	32*	0.81 %	0.26
Total CO_2 [g/kWh]			202

We can estimate the equivalent carbon emissions an electrical vehicle has using the average for carbon dioxide emissions per kilowatt hour of electricity produced. This value depends greatly on how much of the electricity is produced using fossil fuels and as such this calculated average value of 202 g/kWh can only be used as a reference when calculating the equivalent consumption of an electrical vehicle in Finland. Several countries have future plans to utilize wind power in charging the car batteries which simultaneously form country wide electric energy storages for peak shaving. If wind power could efficiently be utilized in electric cars CO_2 emissions would be extremely low and they could also help in balancing the whole electricity production so that the need for high emission peak power should be minimized.

We need to take into account electric power transmission losses and vehicle charging and discharging efficiency. These were not taken into account in the tank-to-wheels-efficiency seen in the Table 2.6 and they further reduce the total efficiency of an electric vehicle. Electricity transmission efficiency in Finland is calculated using equation (2) from available data from year 2008 statistics. /3/

$$\eta_{\text{el,trans}} = \frac{E_{\text{el,tot}} - E_{\text{el,loss}}}{E_{\text{el,tot}}} = \frac{83193\ GWh - 3334\ GWh}{83193\ GWh} = 0.9603 \tag{2}$$

In equation (2) $\eta_{\text{el,trans}}$ is the Finnish electric transmission efficiency, $E_{\text{el,tot}}$ is the total electricity produced in Finland in 2008 and $E_{\text{el,loss}}$ is the total transmission loss.

Now we need to calculate the total efficiency of an electric vehicle. Earlier tank-to-wheels efficiency of 87 % is used to represent the efficiency of the electric power train. For battery charging efficiency an estimate of 91 % was used. This estimate was calculated from charger efficiency of 95 % and from battery charging efficiency of 96 %. If we take into account the discharge efficiency of 96 % the total full cycle battery efficiency is 93 %. Efficiency for actual energy production including fuel production is difficult to assess but a widely accepted estimate of 40 % for electricity generation from varying resources was used. Possibilities and benefits of electricity cogeneration were not taken into account in this estimate. With them the actual efficiency is remarkably higher as only 40 % of the emissions are related to electricity and 60 % to heat, e.g. for district heating.

$$\eta_{\text{ev,wtw}} = \eta_{\text{ev,ttw}} \cdot \eta_{\text{ev,batt}} \cdot \eta_{\text{el,trans}} \cdot \eta_{\text{el,prod}} \tag{3}$$

In equation (3) $\eta_{\text{ev,wtw}}$ is the total well-to-wheels efficiency of an electric vehicle, $\eta_{\text{ev,ttw}}$ is the tank to wheels efficiency, $\eta_{\text{ev,batt}}$ is the battery charge efficiency and $\eta_{\text{el,prod}}$ is the estimate for the efficiency of electricity production.

$$\eta_{\text{ev,wtw}} = 0.866 \cdot 0.912 \cdot 0.960 \cdot 0.400 = 0.303$$

$$\eta_{\text{ev,wtt}} = 0.910 \cdot 0.960 \cdot 0.400 = 0.349$$

Resultant total well to wheels efficiency for an electric vehicle is roughly 30 % when using mainly (about 82 %) thermal power plant production. Total emissions per kilometre can be estimated by using the equivalent emissions per kWh obtained in Table 2.6, average consumption per kilometre in kWh and transmission losses as

$$m_{\text{CO}_2,\text{km}} = \frac{202.43\ ^{\text{g}}/_{\text{kWh}} \cdot E_{\text{kWh/km}}}{\eta_{\text{el,trans}}}. \tag{4}$$

In equation (4) $m_{\text{CO}_2,\text{km}}$ is the amount of carbon dioxide produced per kilometre and $E_{\text{kWh/km}}$ is the average consumption of an electric vehicle.

$$m_{\text{CO}_2,\text{km}} = \frac{202\ ^{\text{g}}/_{\text{kWh}} \cdot 0.2\ ^{\text{kWh}}/_{\text{km}}}{0.9603} = 42\ ^{\text{g}}/_{\text{km}}$$

This is over 90 g/km lower than the goal of 130 g/km set by EU for average emissions for new passenger vehicles in 2012 /5/.

A research conducted by Mitsubishi Motor Corporation states that well to tank efficiency in ICE equipped vehicles is 82.2 % for gasoline and 88.6 % for diesel engines /6/. This is twice higher than that of electric vehicles. While the actual drive train and associated systems efficiency is far greater in electric vehicles powered mostly by thermal power plans and ignoring the heat consumption. Of course, if we could utilize wind or hydro power alone in powering electric cars the situation should be totally changed. The Achilles heel the electric vehicles have is the relatively low efficiency of generation of electricity in thermal power plants. Of course, combi cycles offer higher electricity generation efficiencies up to about 60 %. For example, a gas turbine cascaded with a waste heat steam process produce together in principle 40 % + 0.60 · 40 % = 64 %.

Such plants are, however, rare so far but as the importance electricity is becoming more and more dominating such conversion processes should improve the electricity output remarkably. By shifting the production of electricity from coal and oil-based generation to nuclear, hydro and wind generation the equivalent emissions from electric vehicles become practically nonexistent. So, the above calculated figures give almost the worst scenario in Finland.

In cogeneration the heat that is lost in condensing generation of electricity is put to use. When calculating equivalent emissions for cogeneration of electricity the actual emissions that come from the generation of electricity can be estimated by multiplying the total emissions by the efficiency of electricity generation. As the waste heat is almost fully recovered the rest of the emissions can be delegated to the generation of usable heat.

While the goal of this thesis is not to examine the emissions of electric vehicles or their comparison to combustion engine vehicles, their environmental effects are examined to put an emphasis on the importance of continued development of related technologies and infrastructure. It should be noted that while electric vehicles do not produce local emissions, they do produce carbon dioxide emissions as a byproduct of generation of electricity that are comparable to those produced by ICE equipped passenger vehicles.

As it was mentioned above, it is, however, possible to significantly improve the electricity production efficiency by utilizing most modern thermal power plant technology as the pressure to reduce emissions is constantly increasing and the need for heat is decreasing e.g. when the impact of low-energy or passive energy or even plus energy housing increases. Using combi-cycles in all the Finnish thermal power plants should improve the 42 g/km CO_2 emissions to about 28 g/km. In Table 2.5 are calculated the emissions from different fuel sources assuming that the combi-cycle generation increases the plant efficiency from 40 % to 60 %.

Table 2.5 Adjusted carbon footprint with assumed 60 % efficiency for thermal power plants (*)

Energy source	Carbon emissions CO_2 [g/kWh]	Percentage of electricity production [%]	Adjusted carbon emissions CO_2 [g/kWh]
Coal	627*	15.17 %	95.1
Oil	173*	0.58 %	1.00
Natural gas	133*	12.84 %	17.1
Wind	23	0.23 %	0.05
Hydro	5	17.50 %	0.88
Nuclear	5	29.17 %	0.58
Biomass	21*	11.67 %	2.45
Peat	213*	8.48 %	18.1
Waste	21*	0.81 %	0.17
Total CO_2 [g/kWh]			135.4

3.   ELECTRIC PROPULSION SYSTEM IN ERA

Voltages lower than 1000 VAC or 1500 VDC are regarded as low voltages according to EU's low voltage directive. According to this, "propulsion voltage" is used about the voltage of the traction system to make a difference between the traditional 12 V protective voltage of cars. Electric propulsion system design in ERA is based on the low voltage and propulsion power systems requirements and restrictions given in the competing vehicle technical specification ver. 6.1. Propulsion voltage systems consists of primary and secondary components and conductors. Primary components are the parts of the electric propulsion system that are directly responsible for generating propelling force whereas secondary components provide support and safety functions for the primary components and for the rest of the vehicle.

Figure 3.1 shows the simplified propulsion voltage system schematic. In latter chapters, each part of the system is examined in greater detail.
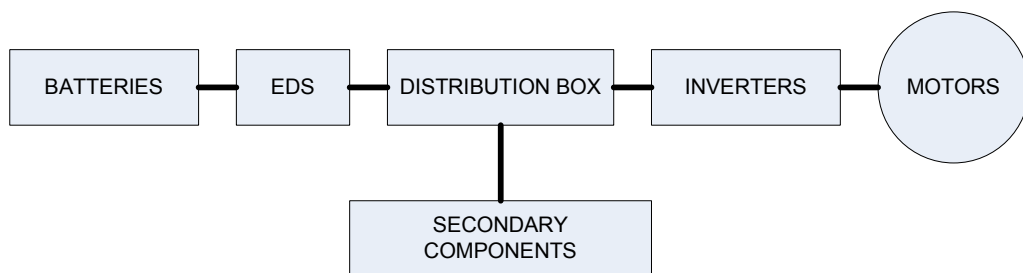

Figure 3.1 Simplified propulsion voltage system schematic

Primary components include batteries, inverters and motors whereas secondary components include DC/DC-converter, two different charging systems, ground fault detection, emergency disconnect switches et cetera.

3.1 BATTERIES

Batteries are the largest single component in the electric system both mass- and volume-wise. In ERA the battery systems consists of two parallel battery packs which each contain 143 Altairnano 50 Ah lithium titanate battery cells. Due to parallel installation of the batteries the total charge of the battery pack is 100 Ah. In Table 3.1 are given the

different voltage values at different operating temperatures and the total voltage available from the battery pack.

Table 3.1 Battery voltages per cell and for the whole pack /7/

Battery	Nominal voltage [V]	Cut-off voltage at -40 °C ±30 °C [V]	Cut-off voltage at +30 °C ±55 °C [V]	Charge cut-off voltage at +20 °C ±55 °C [V]	Charge cut-off voltage at -40 °C ±20 °C [V]
Cell	2.30	1.50	2.00	2.80	2.90
Battery pack	328.90	214.50	286.00	400.40	414.70

In Table 3.1 we can see that the voltage for the whole battery pack ranges from 286 V to 400 V at normal temperature range for temperate climate. However, these values are peak values observed at very low State of Charge (SOC) and at nearly full SOC. To give a more accurate estimate for the average voltage range we need to ignore the voltages at the extremes of SOC-curve. Cell voltage versus SOC is plotted in the Figure 3.2.
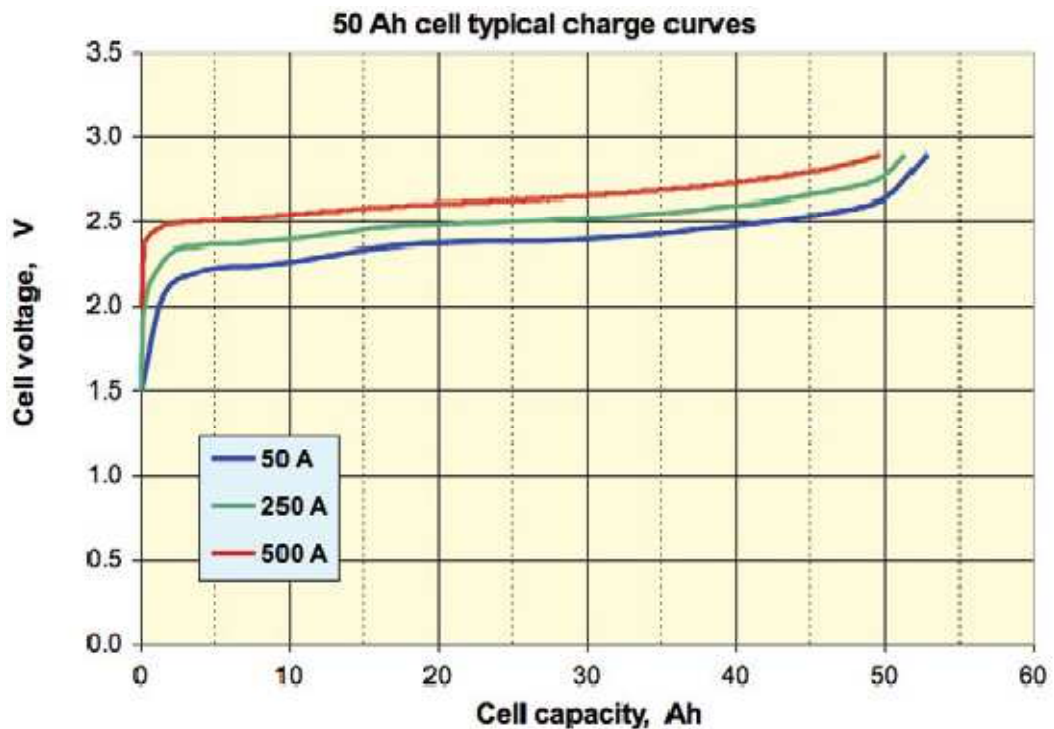

Figure 3.2 Altairnano 50 Ah cell voltage vs. time integral of the charging current /7/

In Table 3.2 are calculated the average voltages while in the linear section of the voltage-SOC-curve. The end-point for the linear section of the curve was estimated to be

50.0 Ah at full SOC and 1.00 Ah, 2.50 Ah and 3.00 Ah respectively for charging currents of 500 A, 250 A and 50.0 A at the low-end of SOC-curve. Cell voltages at these points were estimated to be 2.40 V, 2.30 V and 2.15 V.

Table 3.2 Battery charging voltages

Charging current [A]	Cell voltage at low SOC [V]	Cell voltage at full SOC [V]	Battery pack voltage range min. [V]	Battery pack voltage range max. [V]
50	2.15	2.90	307	415
250	2.30	2.90	329	415
500	2.40	2.90	343	415

Linear sections for discharge voltages were estimated using Figure 3.3. It should be noted that while the voltage curve observed during discharge is similar to the voltage curve seen during charging, the linear section of the voltage curve is shorter during discharge when looking at comparable currents.
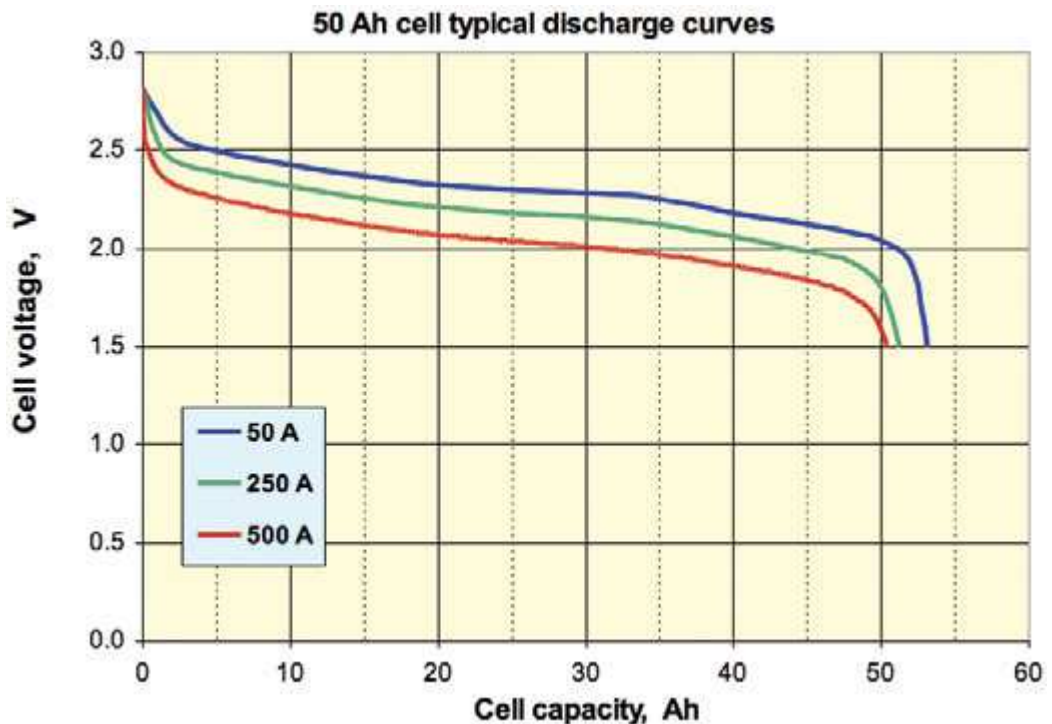

Figure 3.3 Altairnano 50 Ah cell voltages vs. time integral of the discharging current /7/

In Table 3.3 is calculated the linear voltage range apparent during battery discharge.

Table 3.3 Battery discharge voltages

Discharge current [A]	Cell voltage at low SOC [V]	Cell voltage at full SOC [V]	Battery pack voltage range min. [V]	Battery pack voltage range max. [V]
50	2.00	2.60	286	372
250	1.85	2.50	265	358
500	1.70	2.35	243	336

It should be noted that this is the effective voltage range that is available when driving. The maximum and minimum voltages calculated from the values given in the Altairnano 50 Ah lithium titanate cell datasheet are seen only when the SOC of the batteries is either nearly full or almost empty. This is important when looking at the voltage reserve available to the inverters and motors.

3.1.1 Battery capacity and life cycle

As stated in the previous chapter, in ERA the battery systems consists of two parallel battery packs which each contain 143 Altairnano 50 Ah lithium titanate battery cells. Each of the 286 cells is capable of storing 417.6 kJ of energy, thus bringing the total battery pack storage capacity to 119.4 MJ. This is equivalent to 33.2 kWh.

Lithium titanate batteries have a relatively high cycle life of more than 12000 charge-discharge cycles without drastic drop of cell capacity assuming that the battery is otherwise well maintained. Lithium titanate batteries can be repeatedly fully discharged as a part of normal operation without loss of capacity. Manufacturer (AltairNano) promises an expected calendar life of 20 years. Lithium titanate batteries are not subject to shelf-degradation if they are not used for a longer periods of time. /7/

3.2 INVERTERS

Inverters are power electronic devices used to convert DC voltage into AC voltage thus allowing batteries to be used with motors that require three-phase AC. They are identical to frequency converters in design but lack current rectification bridge present in fre-

quency converters due to being connected directly to a DC voltage source. Inverters can alter the frequency of the output voltage magnitude and phase making it possible to use them to precisely control motor currents and performance.

3.2.1 Pulse width modulation with space vector modulation

Inverters use technique called pulse width modulation to create alternating current from direct current. In pulse width modulation each of the output phases is connected to a positive or a negative direct current rail through a semiconductor switch, usually an IGBT. By opening and closing these switches in rapid succession according to the algorithm used a sine-waveform current estimate is produced. How much this output current resembles actual pure sine wave depends on the switching algorithm used, switching frequency and the number of different voltage levels available per output phase.

In Figure 3.4 a basic two-level inverter topology can be seen. There are a total of six IGBTs used as switches and controlled by an inverter software using PWM algorithm as explained later in this chapter. As an individual IGBT is turned either on or off, one of the output phases U, V or W is connected to or disconnected from a DC rail. This results in a voltage transient where line to line voltage changes from 0 volts to either $+U_{DC}$ or $-U_{DC}$.

As the components used in inverters are not ideal, these changes in line to line voltage are not instantaneous but instead real non-zero rise and fall times are observed whenever an IGBT is switched from conducting to non-conducting mode and vice versa. As results, these voltage transients induce high frequency electromagnetic interference components that are either emitted or conducted outwards from the IGBT. This behaviour is examined in greater detail in Chapter 3.5.1.
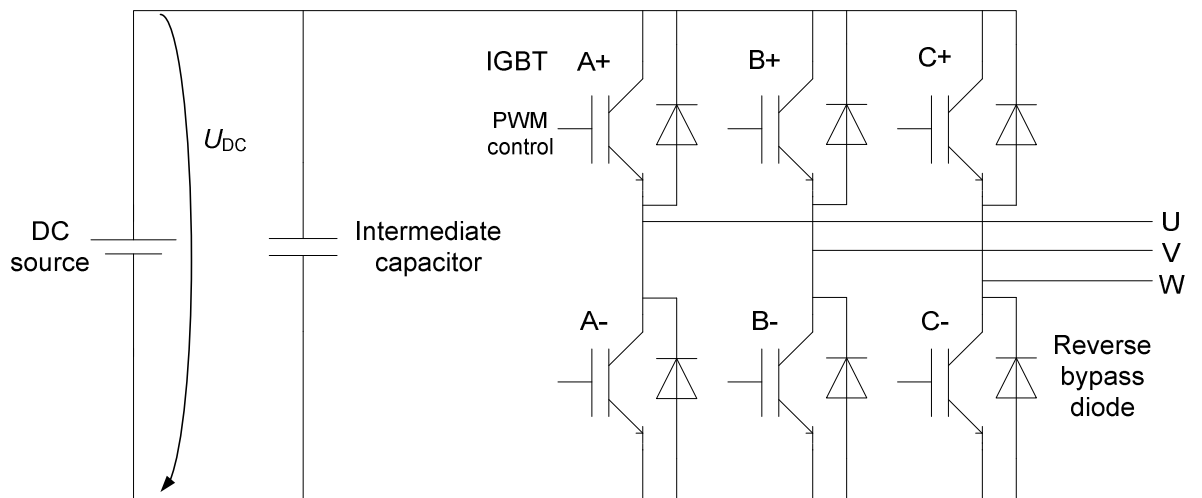
Figure 3.4 Circuit diagram for a three-phase two level inverter

Space vector modulation is an algorithm commonly used in modern inverters to control the pulse-width modulation switching operations. There are varying methods to calculating the switching times and the resultant voltage vector durations but in this thesis space vector modulation is examined only on principle level.

In principle there are a total of $6^2 = 36$ different switch state configurations available when using an inverter with six switches. This number is reduced to eight when switch state configurations resulting in a short circuit between positive and negative rails and other irrelevant combinations are removed. This will happen whenever both A+ and A−, B+ and B− or C+ and C− switches are conducting at the same time. These allowed vectors and their respective switch states are shown in Table 3.4.

Table 3.4 Allowed voltage vectors for two-level inverter

Vector	A+	B+	C+	A−	B−	C−	U_{AB}	U_{BC}	U_{CA}	Vector type
$U_0=\{000\}$	OFF	OFF	OFF	ON	ON	ON	0	0	0	zero vector
$U_1=\{100\}$	ON	OFF	OFF	OFF	ON	ON	$+U_{DC}$	0	$-U_{DC}$	active vector
$U_2=\{110\}$	ON	ON	OFF	OFF	OFF	ON	0	$+U_{DC}$	$-U_{DC}$	active vector
$U_3=\{010\}$	OFF	ON	OFF	ON	OFF	ON	$-U_{DC}$	$+U_{DC}$	0	active vector
$U_4=\{011\}$	OFF	ON	ON	ON	OFF	OFF	$-U_{DC}$	0	$+U_{DC}$	active vector
$U_5=\{001\}$	OFF	OFF	ON	ON	ON	OFF	0	$-U_{DC}$	$+U_{DC}$	active vector
$U_6=\{101\}$	ON	OFF	ON	OFF	ON	OFF	$+U_{DC}$	$-U_{DC}$	0	active vector
$U_7=\{111\}$	ON	ON	ON	OFF	OFF	OFF	0	0	0	zero vector

In space vector modulation each of the eight different allowed switching configurations of a two-level converter results in a specific voltage vector seen in the Figure 3.5. There are six active vectors and two zero voltage vectors. Reference voltage vector U_{ref} is generated by using a dq0-transformation to simplify the three-phased system into a two-axel rotating coordinate system. Once the reference vector is generated, different voltage vectors are switched on for varying durations so that sum of the vectors is equal to the reference vector as

$$\sum_{i=0}^{7} \left(\frac{t_i}{T_s}\right) U_i = U_{ref}. \tag{5}$$

In equation (5) U_i denotes the voltage vector, t_i is the time a corresponding voltage vector is active (switching time) and T_s is the sum of t_i.
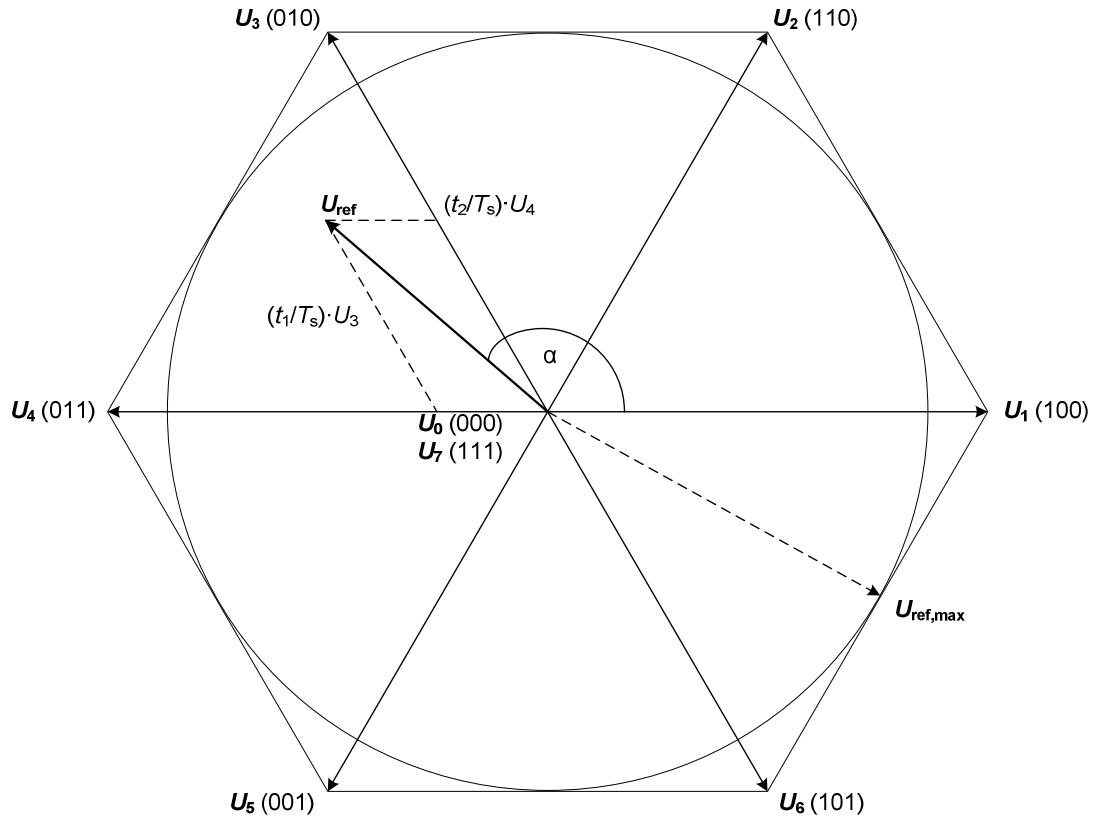
Figure 3.5 Voltage vectors for a three leg converter with $\boldsymbol{U_{ref}}$ and the calculated switching times for two vectors

In Figure 3.5 $\boldsymbol{U_{ref,max}}$ is maximum revolving voltage reference vector static length within linear modulation region whereas hexagon is the linear modulation region. In sine-triangle-comparison based modulation output voltage is directly proportional to modulation index m_a while in the linear modulation region ($m_a \leq 1$). In overmodulation region ($m_a > 1$) amplitude of the fundamental frequency component is no longer linearly dependant on the modulation index. If we increase the modulation index high enough the output voltage will degenerate into square wave form. In vector modulation the modulation index doesn't go above 1.

Maximum RMS line to line voltage ($\hat{u}_{LL,rms}$) within linear operation region ($m_a \leq 1$) can be calculated as

$$\hat{u}_{LL,rms} = \frac{\sqrt{3}}{\sqrt{2}} \cdot m_a \cdot \frac{U_{DC}}{2} = \frac{\sqrt{3}}{2\sqrt{2}} \cdot m_a \cdot U_{DC} \approx 0{,}612 \cdot m_a \cdot U_{DC}. \tag{6}$$

In equation (6) U_{DC} is the direct current voltage fed to the inverter.

In the fully linear region the maximum reference voltage vector stays within the linear operation region at all times. In the high overmodulation region ($m_a \gg 1$) where the output voltage resembles square wave the maximum output line to line RMS voltage can be calculated with

$$\hat{u}_{LL,rms} = \frac{\sqrt{3}}{\sqrt{2}} \cdot \frac{4}{\pi} \cdot \frac{U_{DC}}{2} = \frac{\sqrt{2} \cdot \sqrt{3}}{\pi} \cdot U_{DC} = 0{,}780 \cdot U_{DC}. \tag{7}$$

In the equation (7) multiplier $\frac{4}{\pi}$ is obtained from the Fourier-analysis of the square wave output voltage /8 p. 225-243/.

These values are important as they can be used to calculate the available voltage reserve.

3.3 SECONDARY COMPONENTS

Secondary components are parts of the propulsion voltage system that are not included in the main motive energy production and electricity regeneration cycle but are critical for the operation of the system as a whole, including provision of safety functions. These components include i.e. DC/DC-converter, ground fault detection system, fast charger receptacle, optional slow charger system and different fuses.

3.3.1 Charger

ERA is equipped with two different charger systems. Fast charger receptacle allows the batteries to be charged in minutes to full SOC using external high power charging station. The standard charger allows the batteries to be charged from standard electric outlet. Considerably slower, it takes several hours to fully charge the batteries from 0 % SOC to 100 % SOC using the standard charger system. However, due to lack of fast charging stations at the present time, it is not feasible to rely solely on the fast charger system.

Brusa NLG523-Sx was chosen to act as a slow charger device. It is air-cooled compact modular charger. Using standard 230 V input it can be used to charge battery systems with operating voltages ranging from 260 V to 520 V with maximum charging current of 12.5 A. As a result, maximum charging power is 6.5 kW. To reach 6.5 kW a 40 A fuse is needed. Such single phase 230 V plugs are not commonly available either and a 230 V 16 A plug must be used to reach 2.6 kW charging power. /9/

Using the slow charger system capable of providing 6.5 kW of charging power, the amount of time it takes to fully charge the batteries in ERA can be estimated

$$t_{\text{charge}} = \frac{E_{\text{batt}}}{P_{\text{charger}} \cdot 3600s} = \frac{119,4 \text{ MJ}}{6500 \text{ } W \cdot 3600s} = 5.1 \text{ h.} \tag{8}$$

In equation (8), t_{charge} is the amount of time in hours it takes for the slow charger to fully charge the batteries, E_{batt} is the battery capacity in megajoules and P_{charger} is the charging power. As can be seen from the result, it takes 5,1 hours to fully charge the batteries, a time short enough to allow the batteries to be charged overnight or during normal working day. If instead of a 40 A plug normal 16 A plug is available almost 13 hours are needed to charge the battery.

It should be noted that the slow charger system is an optional system and won't be installed in ERA during preliminary testing and the actual race. Instead, a fast charging solution will be used.

3.3.2 DC/DC Converter

A DC/DC converter is used to provide power 12 V protective voltage system charging. It converts voltage from the batteries into 12 volts used by the protective system. Due to non-existent availability in the required power range and due to the need of quick delivery the only viable option for DC/DC conversion was Brusa BSC624-12V. BSC624 is a buck-boost converter, thus being capable of providing 8-16 volt output voltage over a wide input voltage range of 220 to 450 volts. This is an almost exact fit with the voltage

range provided by the battery pack (286 V - 415 V) depending on the level of charge. /10/

Buck-boost converters have a relatively simple ideal topology seen in Figure 3.6.
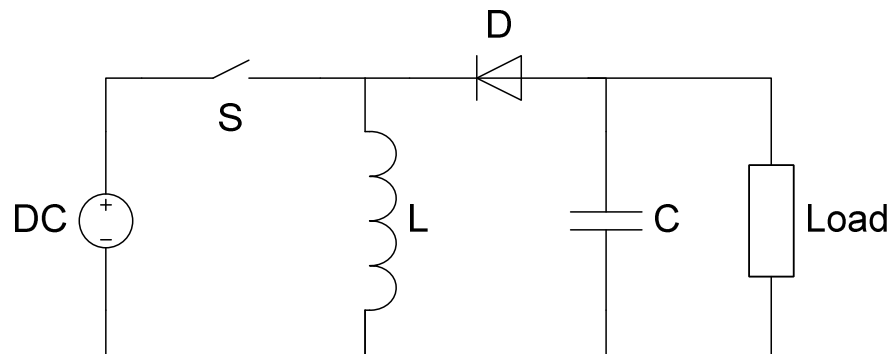

Figure 3.6 Simplified buck-boost converter topology

3.3.3 Ground Fault Detection Unit

Ground fault detection is one of the major safety measures present in the practically every modern commercialized electric vehicle. It is used to detect possible short circuits or resistive conducting connections between current-carrying conductors and the ground level present in the system. Should such a connection be detected, the ground fault detection will inform the driver of the fault current. Driver can then open the EDS relays and disconnect the battery from the rest of the system. This will not immediately de-electrify the system however, as there are inductive and capacitive loads present in the system, mainly in the intermediate circuit capacitors found in the inverters.

A-ISOMETER® iso-F1 IR155-2 is a compact device for monitoring insulation on unearthed DC power supplies. It has several major advantages, one of the greatest being that it was available in due time. Other major benefits include /11/:

- Insulation monitoring for unearthed DC systems 0…800 V
- Automatic adaptation to the existing system leakage capacitance
- Optimized measurement technique for low-frequency control processes

- Connection monitoring to reference earth (vehicle chassis)

Ground fault detection unit behaviour as a part of vehicle electric safety system is examined in Chapter 3.4.

3.4 ELECTRIC SAFETY MEASURES IN ERA

One of the most important goals of this thesis was to design an electric safety system capable of protecting passengers in case of an accident and during faults and maintenance.

One of the concerns related to the battery pack was that the electric neutral point in the middle of the batteries was not mechanically available for installation of additional components or devices. The closest available point electrically is located three fourths towards positive connectors.

During maintenance the battery pack can be isolated by opening manual isolation switch located one fourth from the electric middle point of the battery towards positive connectors. Opening the manual isolation switch also opens the main relay control contactor located in the isolation switch. EDS relays should be open at this point but if they are still closed and unless they are damaged in a way that prevents them from being opened electrically (high current welding, i.e.), they will open when the manual isolation switch is opened. The battery pack, the manual isolation switch, chargers and the EDS and precharge relays are seen in Figure 3.7.
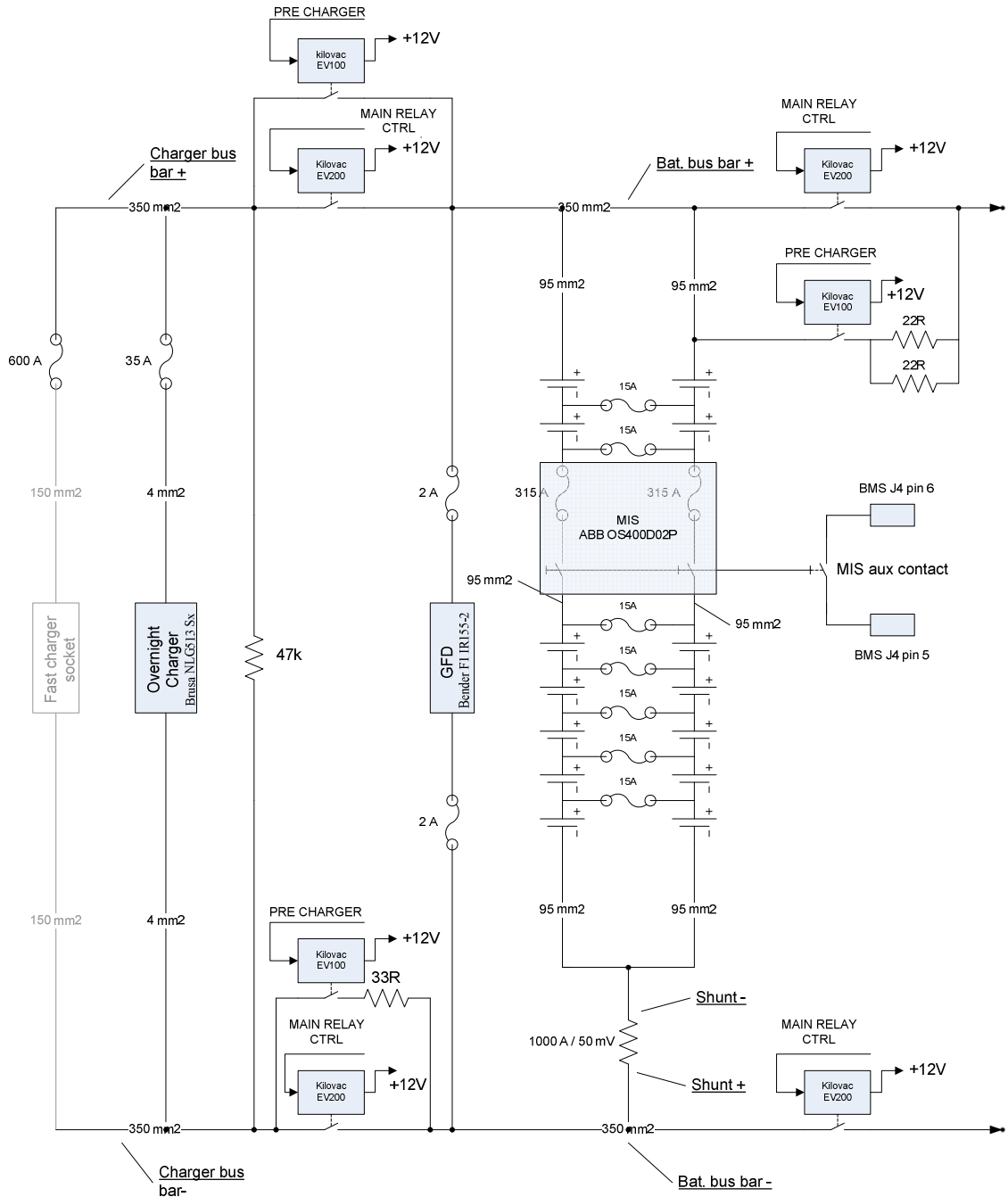
Figure 3.7 Manual isolation switch, the two different chargers, emergency disconnect and precharge relays

Emergency disconnect relays are controlled by the main relay control signal, drawn in the schematic as a "MAIN RELAY CTRL" signal path. Kilovac EV200 relays are capable of disconnecting loads up to 360 kW (900 A at 400 V DC) at least 10 times before failure. For redundancy and added safety two EDS relays were used at both positive and negative ends of the battery pack. Inverter intermediate capacitors are charged through

relays Kilovac EV100 prior to switching the EDS relays on. This helps to prevent a large charging current inrush that would otherwise occur whenever the main EDS relays are switched on and the intermediate capacitors are not charged. /12/

EDS relays are normally open-type relays. When one of the switches on the main relay control signal path seen in Figure 3.8 is opened the EDS relays are opened. Ground fault detection unit is connected to the main vehicle computer and in case it is triggered, EDS CONTROL signal drops to 0 volts. Physical switches controlling the EDS relays are two emergency shutdown buttons located in the cockpit and on the rear right window, normally closed-type inertia switch and the contactor located in the manual isolation switch. Should any of these trigger, the EDS relays will open and isolate the batteries from the rest of the system.
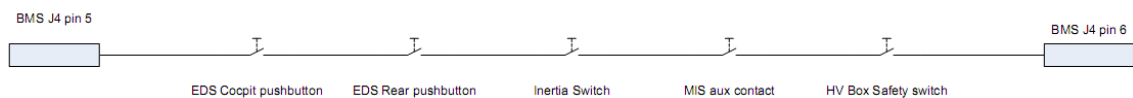

Figure 3.8 Main relay control signal path

The inertia switch will trigger and open when the vehicle is subjected to acceleration or deceleration in excess of 9 g.

All of conductors and thus all of the components are protected by fuses located either in the distribution box or in the battery middle point. Fuse ratings are designed to allow the devices to operate at their maximum rated current. Fuse ratings and their descriptions can be seen in Table 3.5.

Table 3.5 Fuse ratings and descriptions

Fuse designation in schematic	Fuse desciption	Conductor max. current rating [A]	Fuse rating [A]	Fuse location
PWM FUSE1-4	Inverter and motor fuses	300	325	Distribution box
DC/DC CONVERTER FUSE	DC/DC converter fuse	16	35	Distribution box
FAST CHARGER FUSE	Fast charger vehi-cle-side fuse	600	600	Distribution box
SLOW CHARGER FUSE	Slow charger fuse	35	35	Distribution box
GFD FUSE1-2	Ground fault detec-tion unit fuse	0,5	2	Distribution box
BATTERY FUSES	Battery fuses	500	525	Battery mid-dle point

3.5 EMC

Electromagnetic compatibility is a major concern in all modern electronic applications. Especially, in a relatively small vehicle where there are several high-power electronic devices and conductors located in close proximity to sensitive 12 V systems and wiring.

Electromagnetic interference (EMI) is the disruption of operation of an electric device due to emitted electromagnetic radiation or conducted electromagnetic signal from an another electric device operating in the vicinity. This disturbance may be harmless but on the other hand, it may cause the device to cease from functioning while it is under the effects of interference, cause it to degrade and age faster or destroy the device alto-gether.

Most often electromagnetic interference is caused by rapidly changing currents often found in power electronic devices such as inverters and converters but also they caused by natural phenomena such as lightning strikes or the radiation emitted from the Sun.

Fast changes in both voltages and currents within a switching converter cause the inverter to act as a source for EMI. On the other hand, the converter itself suffers from the interference it has caused itself. The interference is transmitted in two ways, through radiation and through conduction. Conducted interference is divided into two kinds of subcategories of noise, common mode and differential mode noise.

Common mode noise is measured between the power lines and ground whereas differential mode noise is measured between power lines. In Figure 3.9 the transmission of common mode and differential mode noise originating from the inverter through stray capacitances is shown. CM and DM noise is also generated in the motor and transmitted from off the drawn circuit, but for sake of clarity their paths are not shown in the Figure 3.9.
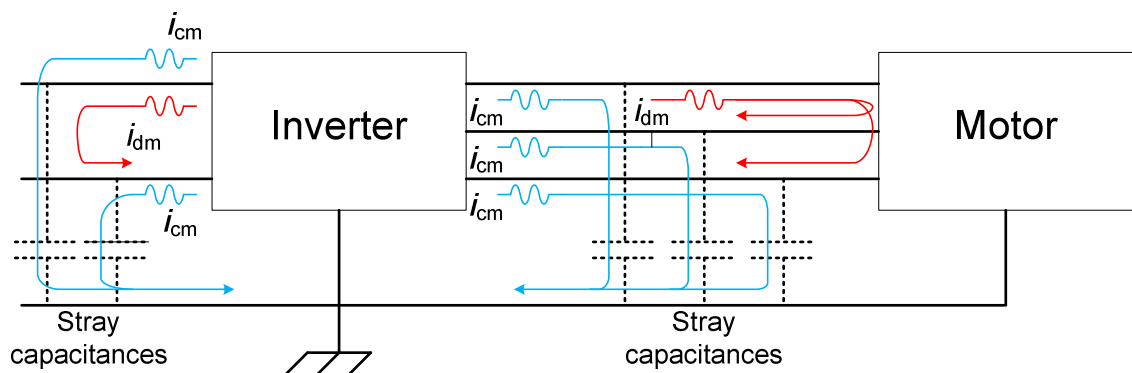

Figure 3.9 Transmission of common mode and differential mode noise through stray capacitances

The best way to handle EMI would be to prevent them from being generated at the source, but since this is not an option different ways of managing with existing interference will be examined. Radiated emissions are relatively easily contained by building a Faraday cage around the components and devices prone to cause or suffer from EMI. /13/ /14/

3.5.1 IGBTs As Sources Of EMI

Non-zero rise and fall times observed in non-ideal IGBTs give rise to du/dt and di/dt phenomena where either voltage or current changes rapidly. This causes high frequency

components to appear on the conductors and on the ground plane. Observed frequency is directly related to the inverse of t_r, the rise time, and t_f, the fall time, of the voltage or current when the transistor is switched on or off. This relation is described by /15/

$$f_{BW} \approx \frac{1\,s}{\pi \cdot t_r}. \tag{9}$$

In Figure 3.10 the difference between an ideal and real IGBT can be seen. Dotted line shows the ideal switching voltage waveform whereas solid line shows voltage behaviour of a real IGBT with voltage overshoot.
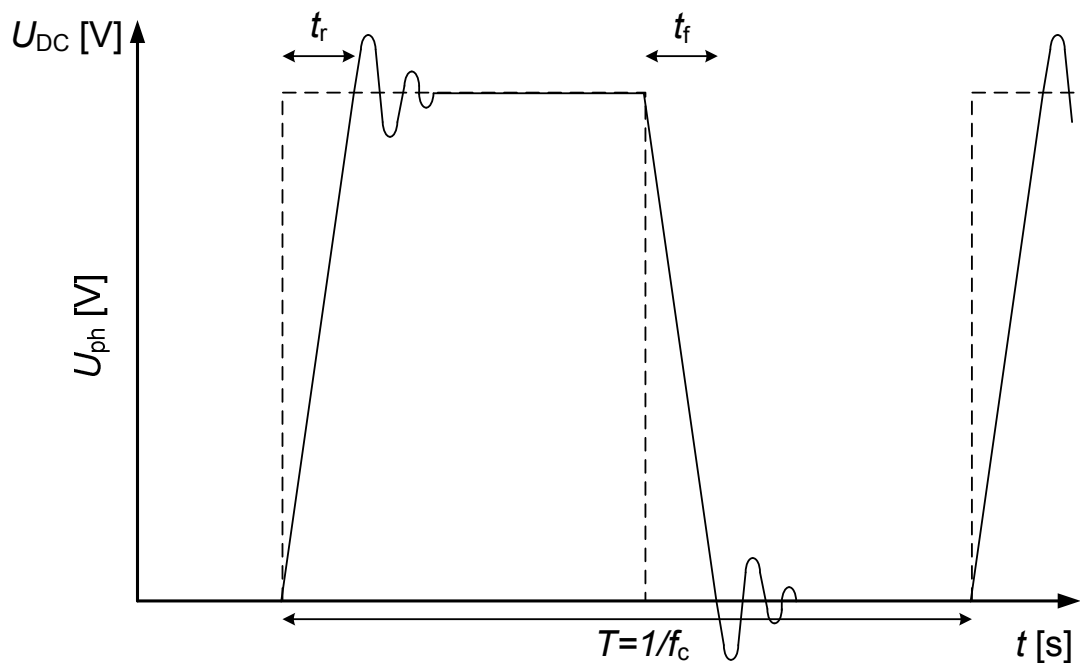

Figure 3.10 Ideal (dotted) and real (solid) voltage waveforms of an IGBT /11/

In Figure 3.11 the differential mode voltage amplitude is plotted as a function of frequency. As can be seen the amplitude experiences little or no attenuation at all until the switching frequency f_c. At frequencies higher than the switching frequency the amplitude attenuates 20 dB/decade. At frequencies higher than the bandwidth frequency f_{BW} the amplitude attenuates at 40 dB/decade. /15/ /16/
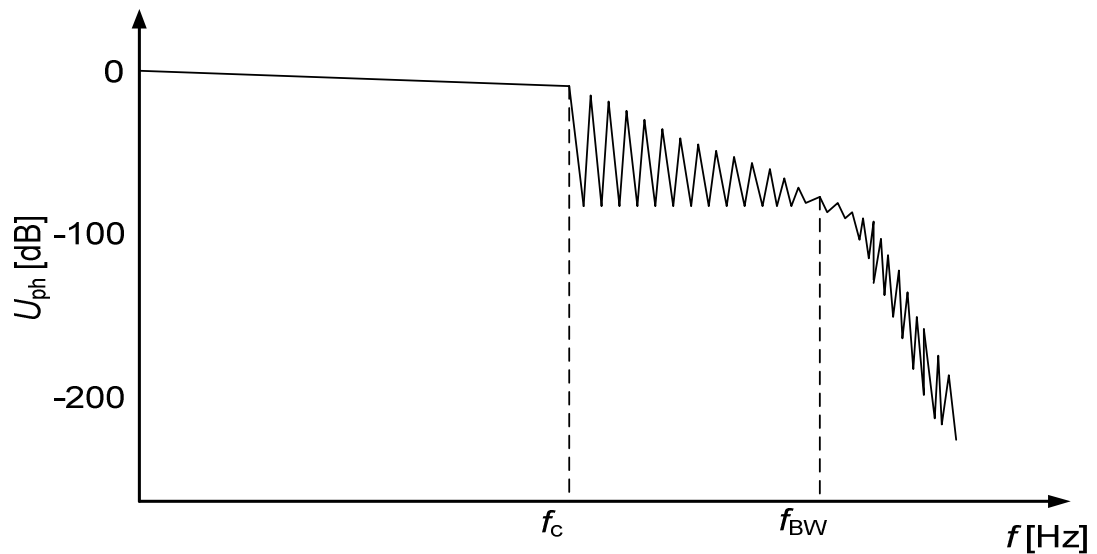
Figure 3.11 Voltage amplitude vs. frequency /11/

Modern IGBTs are capable of reaching switching times of 40 ns and less. Some of the most common commercially available IGBTs, their switching times and frequency of the resultant interference components are listed in Table 3.6. /16/

Table 3.6 Rise and fall times for several commercially available IGBT and related bandwidths

Manufacturer	Part #	Typical rise time t_r [ns]	Typical fall time t_f [ns]	Estimated bandwidth for t_r and t_f [MHz]	
Dynex Semiconductor	DIM200WBS12	95	50	3.4	6.4
Microsemi	APT102GA60B2	37	101	8.6	3.2
Fairchild Semi	FGA180N33ATD	80	250	4.0	1.3
Semikron	SKM100GB125DN	40	20	8.0	15.9
Infineon	FS200R06KE3	30	60	10.6	5.3

3.5.2 Inverters EMC-wise

Inverters are the single greatest source of electromagnetic emissions in the propulsion voltage system in ERA. This is due to the high voltage transients native to pulse width modulation-based frequency control and non-idealities of IGBTs switching at high frequencies. As there is no way to prevent the generation of these EM emissions, it is im-

portant that we minimize the radiation leakage by shielding the inverter and the conductors connecting the inverters to the motors. /13/

Inverters themselves are fully enclosed with conducting material to prevent any leakage of emissions but the original design of the inverters had the inverter sides covered with aluminium but left the inverter ends open to electromagnetic emissions as the ends were sealed with a non-conducting plastic material. This also prevented cables from being properly shielded as the shielding could not be extended at the inverter end to give the cable shield a 360° contact with the inverter casing.

Figure 3.12 shows the original unmodified inverter cable feed end. As can be seen the inverter case is sealed in the cable feed end with a plastic material and neither the DC cables, motor feed cables or the CAN-control cables are shielded nor could the shielding be properly grounded to the inverter chassis even if they were.
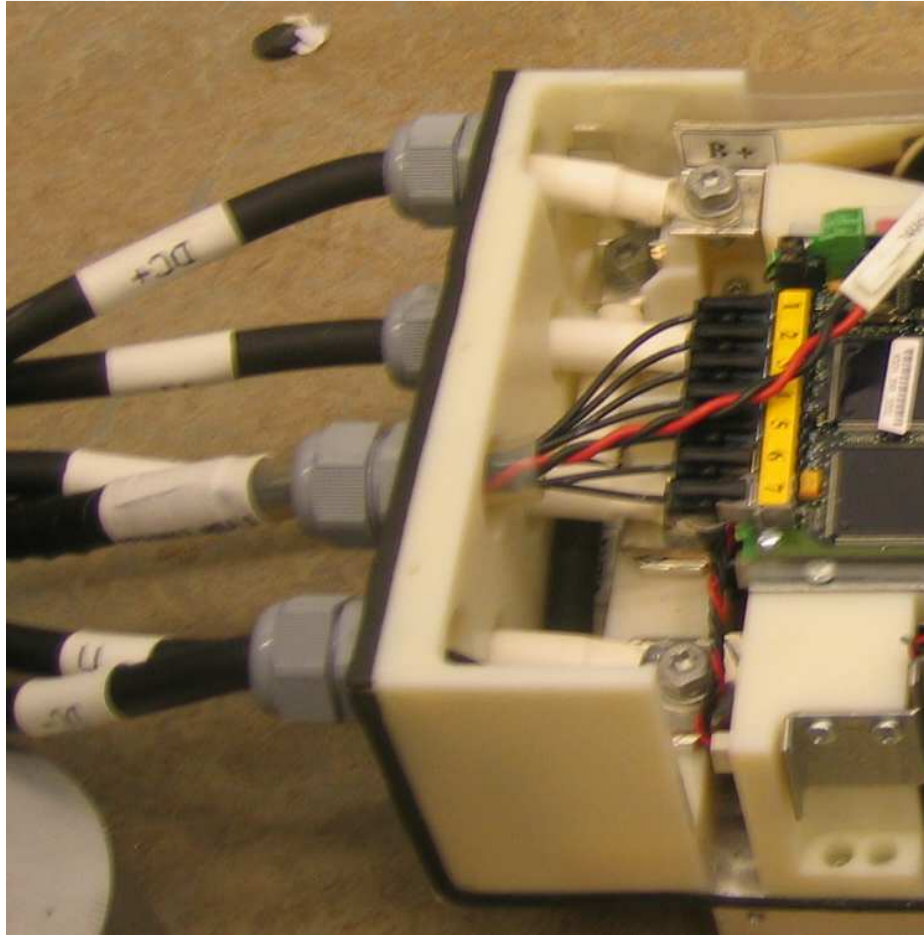
Figure 3.12 Vacon NXP special inverter original plastic cable feed end

To rectify this problem the inverter casing was modified to fully cover the inverter with aluminium. This also made it feasible to use EMC compliant cable feed-through conduits. For this purpose SKINTOP® MS-SC-M was chosen. It offers 360˚ contact between the cable shielding and the inverter case thus effectively eliminating any leakage emissions from the inverter or from the cables from passing on to nearby devices or wires. Figure 3.13 shows cross-section image of the SKINTOP® MS-SC-M with established connection to the cable shielding.
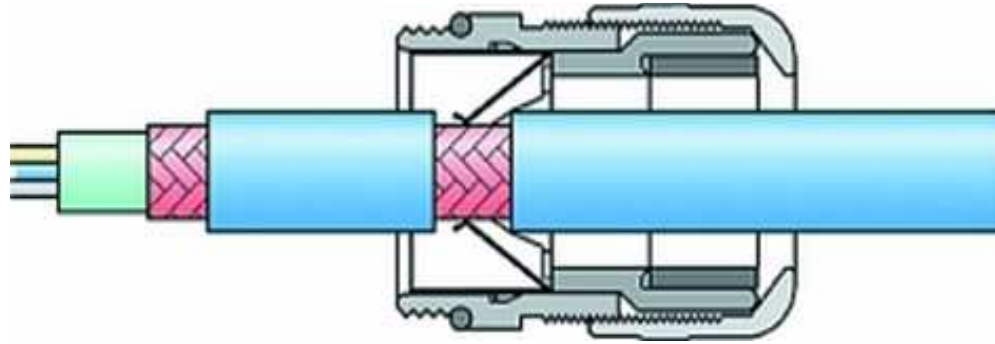
Figure 3.13 SKINTOP® MS-SC-M cable feed through conduit cross-section image /17/

In Figure 3.14 the main proposed methods of minimizing electromagnetic emissions, both emitted and conducted, are shown. They are:

a) DC-input cables are fully shielded

b) Input cables are wound through a ferrite ring to eliminate common mode noise

c) Cables are brought into the inverter through SKINTOP® MS-SC-M cable feed through conduits

d) Three motor output cables leave the inverter through SKINTOP® MS-SC-M cable feed through conduits

e) Ferrite rings around motor cables at the inverter end to minimize common mode currents /17/

f) SKINTOP® MS-SC-M feed through conduits are used to connect the shielded cables to the motor
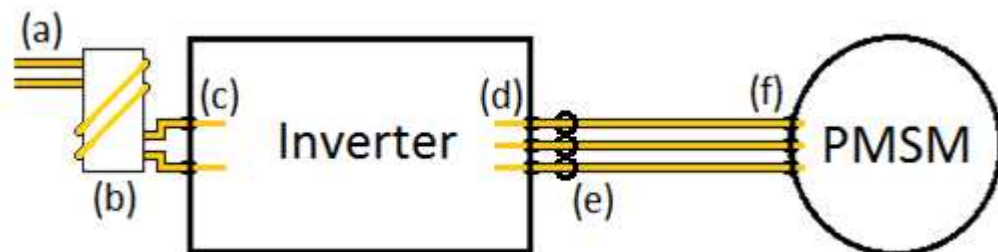

Figure 3.14 Inverter-motor couple EMC design

This seamless conducting shielding creates a Faraday cage around the inverter-motor pair, effectively eliminating radiated EMI emissions emitted from the inverter-motor pair. /13/

Conducted EMI is transmitted through parasitic capacitances wherever there is a dielectric material between two conductors in different electric potential. /13/ /14/

3.5.3 DC/DC Converter EMC-wise

Most common switches found in converters are IGBTs or other semiconductor power electronic switches. While otherwise well suited for use in power electronic devices, IGBTs are real components and thus switching operation is not instantaneous, this was covered in. This results in non-zero rise- and fall times seen in the voltage. This in turn creates high frequency electromagnetic interference components. While the actual unit could not be tested or measured, emitted and conducted interference was estimated using an image found in the BSC624 manual. These rising and falling edge estimates can be seen in Figure 3.15 as thin red vertical lines. /10/
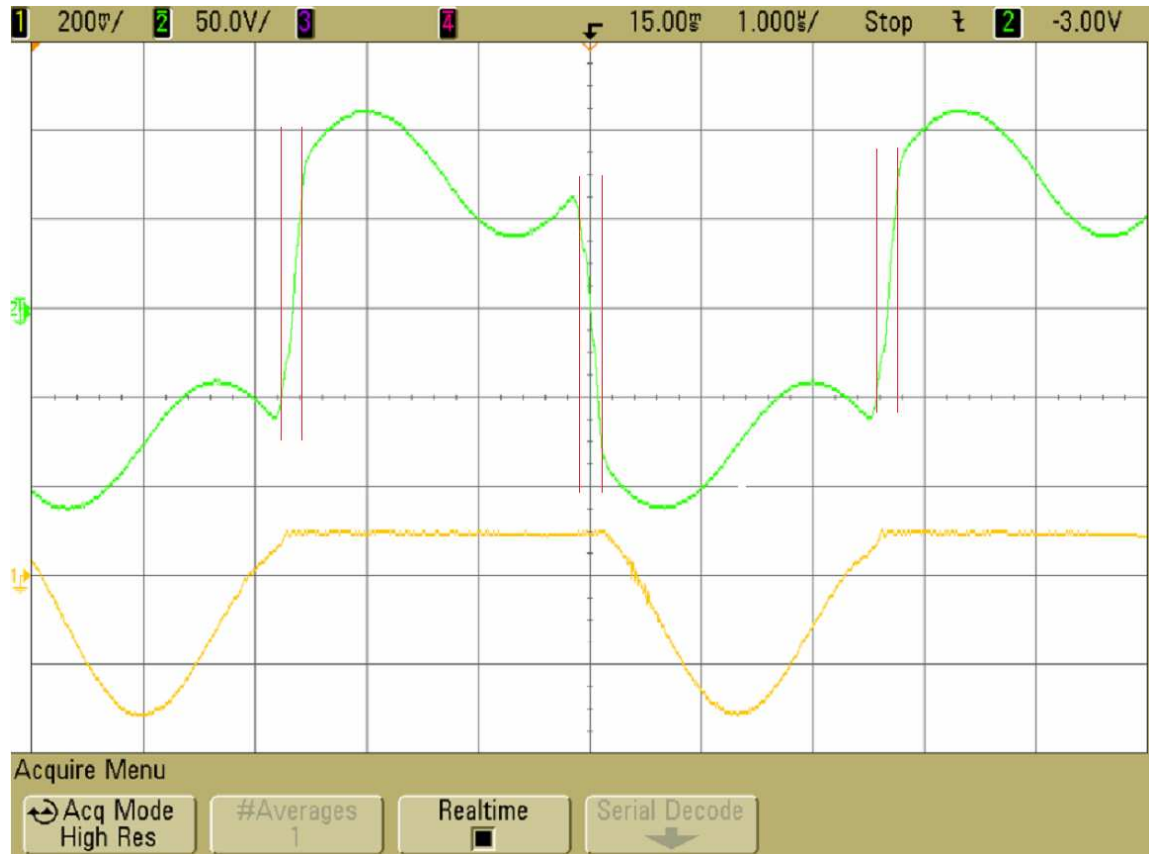
Figure 3.15 Estimates for rise and fall times

From these estimates we can calculate the expected highest frequency components found in the emitted electromagnetic noise using

$$f_{\text{conv,emi(max)}} = \frac{1\text{s}}{\pi \cdot t_{\text{r}}} = \frac{1\text{s}}{\pi \cdot 1 \mu s \cdot {}^{22}/_{144}} = 2.083 \text{ MHz.} \tag{10}$$

In equating 10 ${}^{22}/_{144}$ is the width of the rise/fall time estimate divided by the width of one microsecond in pixels. These were obtained in Figure 3.15. Main wave form seen in Figure 3.15 as a green line corresponds to a frequency of 185 kHz, which is just short of the highest stated occurring switching frequency of 189 kHz found in the converter in galvanic isolation transformer /10/.

3.6 EFFICIENCY AND LOSSES IN THE ELECTRIC PROPULSION SYSTEM

In this chapter the efficiency and losses present in the electric propulsion system are examined. As there is no test data available due to the late delivery of the battery pack, an estimate was calculated using available data from cell technical specification. Only the losses on the primary components are examined as their load varies only depending on the load on the motors. Secondary components produce negligible losses when compared to the components on the drive train or they occur when the vehicle is being charged, thus not affecting the total efficiency when driving.

3.6.1 Batteries

Each cell has an internal resistance of 0.55 mΩ at cell voltage <2.8 V, thus the total resistance of the two parallel 143 cell battery packs can be calculated as /7/

$$R_{\text{tot,batt}} = \frac{R_{\text{pack}}}{2} = \frac{143 \cdot 55 \cdot 10^{-4} \Omega}{2} = 39 \text{ m}\Omega. \tag{11}$$

In equation (11) $R_{\text{tot,batt}}$ is the total resistance of the two parallel battery packs and R_{pack} is the resistance of a single battery pack consisting of 143 individual cells connected in series.

Output power and losses were calculated. As seen in Table 3.**3** the output voltage U_{batt} depends on the output current I_{batt}. To give a more accurate estimate of the output power $P_{\text{out,batt}}$ the output voltage was linearized as a function of output current.

$$P_{\text{out,batt}} = U_{\text{batt}} \cdot I_{\text{batt}} \tag{12}$$

$$P_{\text{loss,batt}} = I_{\text{batt}}^2 \cdot R_{\text{tot,battery}} \tag{13}$$

Depending on the load on the motors, a current of varying amplitude is drawn from the battery pack. Losses caused by the internal resistance of the battery pack are plotted against the amplitude of the current in Figure 3.16. As can be seen in the Figure 3.16 the losses increase rapidly as the current increases whereas the total output power grows more linearly.
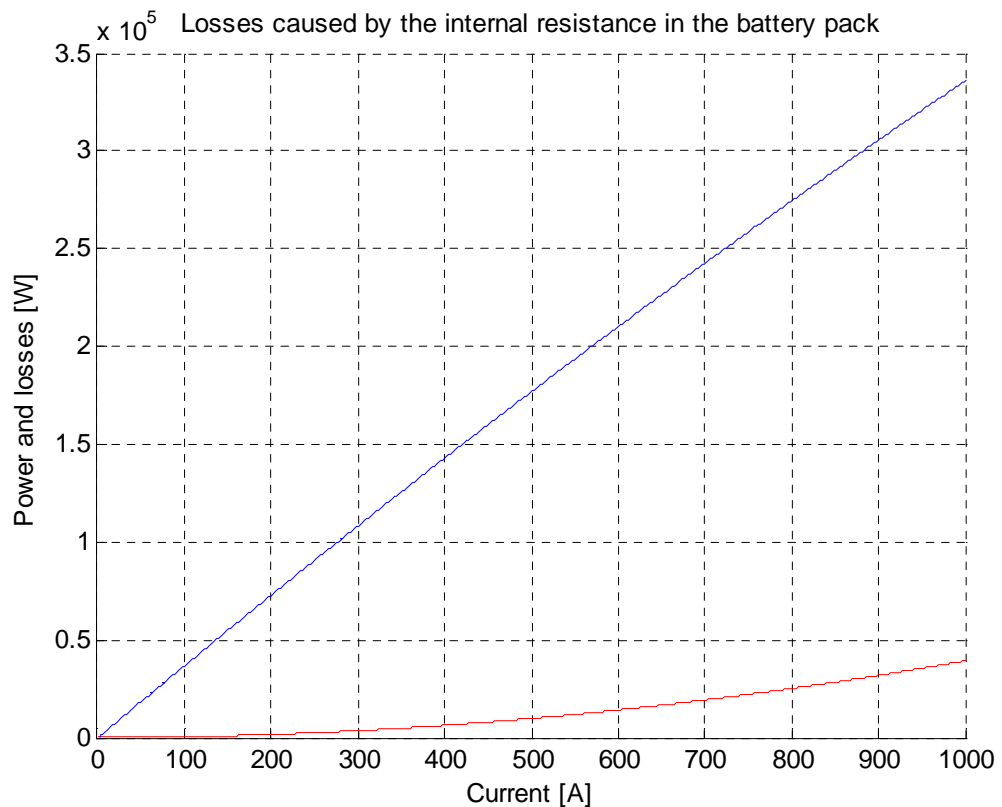

Figure 3.16 Output power (blue) and losses (red) in the battery pack

The internal resistance also causes a voltage drop in the battery pack linearly dependant on the current. This causes the output voltage U_{batt} to drop as the output current I_{batt} increases. This voltage drop can be calculated as

$$U_{\mathrm{drop,batt}} = I_{\mathrm{batt}} \cdot R_{\mathrm{tot,battery}}. \tag{14}$$

During normal operation where output current ranges from 50 A to 400 A the total voltage drop ranges from 2 V to 16 V at 400 A. At 1 kA output current the total voltage drop is 39 V.

As can be seen in Figure 3.16 the losses in the battery pack increase rapidly as the current rises. If we consider the nominal fast charging current of 600 amperes, this would translate as ~14 kW of thermal losses that would have to be dissipated to prevent battery from overheating and from being permanently damaged.

3.6.2 Conductors

Conductors are passive components that cause losses due to their non-ideal nature. This non-ideality manifests as resistivity, which causes the conductor to resist the flow of current.

In ERA all the conductors are made of copper, which is one of the best conductors in regard to resistivity. Resistance of a conductor can be calculated according to Ohm's law as

$$R_{\mathrm{cond}} = \rho \cdot \frac{l_{\mathrm{cond}}}{A_{\mathrm{cond}}}. \tag{15}$$

In equation (15) R_{cond} is the resistance of a conductor, ρ is the material specific resistivity, which for copper is 16.78 nΩm at room temperature, and A_{cond} is the cross-sectional area of the conductor. Resistances of the conductors found in the current path between batteries and motors are calculated in Table 3.7. Conductor cross-sectional areas were chosen according to principle of 3 A of nominal current per mm^2. All conductors are PVC-insulated and can withstand operating temperatures of 125 °C for extended periods of time.

Table 3.7 Conductor resistances

Conductor	Conductor area [mm^2]	Conductor length [m]	Conductor resistance per meter [μΩ]	Total conductor resistance [mΩ]
Battery - EDS	120	8	139.83	1.12
EDS - Distribution box	185	2	90.70	0.18
Distribution box - Inverter	40	16	279.67	10.07
Inverter - Motor	35	12	479.43	5.75
Distribution box - Fast charger	150	2	111.87	0.22

In Table 3.7 the conductor length also accounts for the cases where there are multiple parallel conductors of same cross-sectional area.

In Table 3.8 he losses arising from the inherent resistivity of the copper conductors are calculated. As can be seen they are borderline negligible when compared to the losses found in the primary components.

Table 3.8 Conductor losses

Conductor	Nominal current [A]	Total conductor resistance [mΩ]	Resistivity losses on nominal current [W]
Battery - EDS	300	1.12	100.68
EDS - Distribution box	600	0.18	65.31
Distribution box - Inverter	80	10.07	64.44
Inverter - Motor	100	5.75	57.53
Distribution box - Fast charger	600	0.22	80.54

3.6.3 Inverter and Motor Efficiency

According to the inverter operating manual and technical specification, the inverters operate at 97 percent efficiency whereas the motor operates at 95 % nominal efficiency. Combined, the total efficiency for inverter - motor pair is 92.15 % not including the losses present in the cables connecting the inverter to the motor. These figures are, however for the rated operation of the components and, in practice, lower efficiencies will be seen at partial loads and in overload. /18/ /19/

3.6.4 Energy Consumption

Assuming no losses in the power train, the only major factors affecting the energy consumption of the vehicle propagating at constant velocity are air resistance of the vehicle (drag) and rolling friction of the tires. Air resistance and rolling friction can be calculated as

$$F_{\text{air}} = \frac{1}{2} \cdot \rho \cdot v^2 \cdot C_{\text{d}} \cdot A_{\text{ref}}. \tag{16}$$

In equation (16) F_{air} is the force of the drag, ρ is the density of the air, C_{d} is the form-dependant drag coefficient and A_{ref} is the reference area of the vehicle (area of the vehicle cross-section perpendicular to the direction of flow of the air).

$$F_{\text{fric}} = C_{\text{rr}} \cdot m \cdot g \tag{17}$$

In equation (17) F_{fric} is the rolling resistance, C_{rr} is the rolling resistance coefficient, m is the mass of the vehicle and g is the gravitational constant.

Assuming that C_{d} is 0.32, A_{ref} is 1.76 m^2, ρ is 1.2 kg/m^3, C_{rr} is 0.01, m is 1800 kg and g is 9.81 m/s^2 the resultant forces of drag and rolling friction are plotted against vehicle speed v in Figure 3.17.
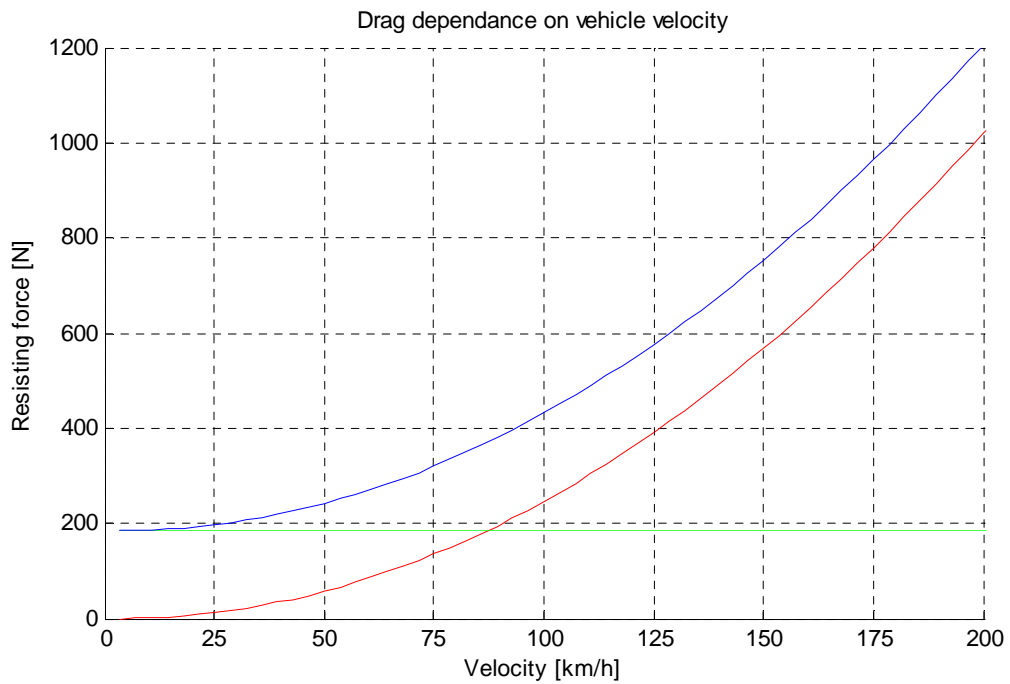
Figure 3.17 Resisting forces (drag - red, rolling friction - green and total resisting force - blue) and vehicle speed

At a velocity of 100 km/h the force resisting motion of the vehicle is 431 N (Figure 3.17) and thus total energy consumption per kilometre is 431 kJ (120 Wh).

Using the tank-to-wheels efficiency of 0.866 for electric vehicle calculated in Chapter 2.2 the total consumption per kilometre is 139 Wh/km. During testing it was found out that the average consumption when driving at 80 km/h is 190 - 200 Wh/km, thus the additional energy required is 60 Wh/km. Considering the case that this consumption is caused solely by the secondary components, the total power drawn by secondary components is 60 Wh/km · 80 km = 4.8kW. It should be noted that the power drawn by the secondary components does not vary depending on speed, thus the added consumption of electric energy per kilometre depends inversely on vehicle speed.

4. RELUCTANCE-AIDED PERMANENT MAGNET SYNCHRONOUS MOTORS

Perhaps the most defining element of an electric vehicle is the electric motor propelling the vehicle. Motive force generation in ERA is done using four permanent magnet synchronous motors, one for each wheel, each controlled with a three-phase PWM inverter described in Chapter 3.2. This allows for superior per-wheel control during driving and increased safety as each wheel can be controlled precisely and quickly when the need arises.

4.1 PERMANENT MAGNET SYNCHRONOUS MOTORS

PM synchronous reluctance motor such as the motors used in ERA generate torque through interaction between the flux produced by the permanent magnets, reluctance-wise nonsymmetrical rotor and the current in the armature. In contrast to other types of electric motors, in permanent magnet motors, although the shaft output power is zero, there already exist a flux caused by the permanent magnets and the difference between direct-axis and quadrature inductances. One of main factors holding permanent motors from becoming de facto motors for vehicle applications is the lack of high-remanence magnetic materials with suitable mechanic properties. Most of the high-remanence magnetic materials have either low Cúrie temperature or brittle and hard ceramic composition.

In Figure 4.1 the permanent magnet motors found in Toyota Prius 2003 and 2004 models can be seen. 2004 model has its windings connected in series instead of two-parallel windings of 2003 model.

Figure 4.1 Prius 2003 and 2004 permanent magnet motors /19/

4.1.1 Torque Generation in PMSM

As stated in the previous chapter, torque generation in PMSM is achieved through inter-action between stator flux and the flux generated by the permanent magnets in the rotor. If the rotor is not symmetrical reluctance-wise, reluctance torque will have considerable effect on the total torque produced. Torque can be estimated as /21 p. 9.6-9.9/ /22/

$$T = 3 \cdot \frac{p}{\omega_s^2}\left(\frac{U_{sv}\cdot E_{PMv}}{L_d}\sin\delta + U_{sv}^2\frac{L_d-L_q}{2\cdot L_d\cdot L_q}\sin2\delta\right). \tag{18}$$

Power can be estimated as /21 p. 9.6-9.9/ /22/

$$P = T \cdot \frac{\omega_s}{p} = \frac{3}{\omega_s}\left(\frac{U_{sv}\cdot E_{PMv}}{L_d}\sin\delta + U_{sv}^2\frac{L_d-L_q}{2\cdot L_d\cdot L_q}\sin2\delta\right). \tag{19}$$

T is the torque produced, P is the power produced, p is the pole-pair number of the ma-chine, U_{sv} is per-phase stator voltage, E_{PMv} is per-phase back emf, ω_s is stator electric angular velocity and L_d and L_q are direct- and quadrature-axes inductances. Reluctance torque, which is dependent on the difference between L_d and L_q, is the second term in equations (18) and (19). As it can be seen the reluctance torque will appear as the sec-ond harmonic when torque produced is plotted against the mechanical load angle of the machine. This behaviour is shown in Figure 4.2 (torque) and in Figure 4.3 (power).

Green in the reluctance component, red is the electromagnetic component and blue is the sum of the former.
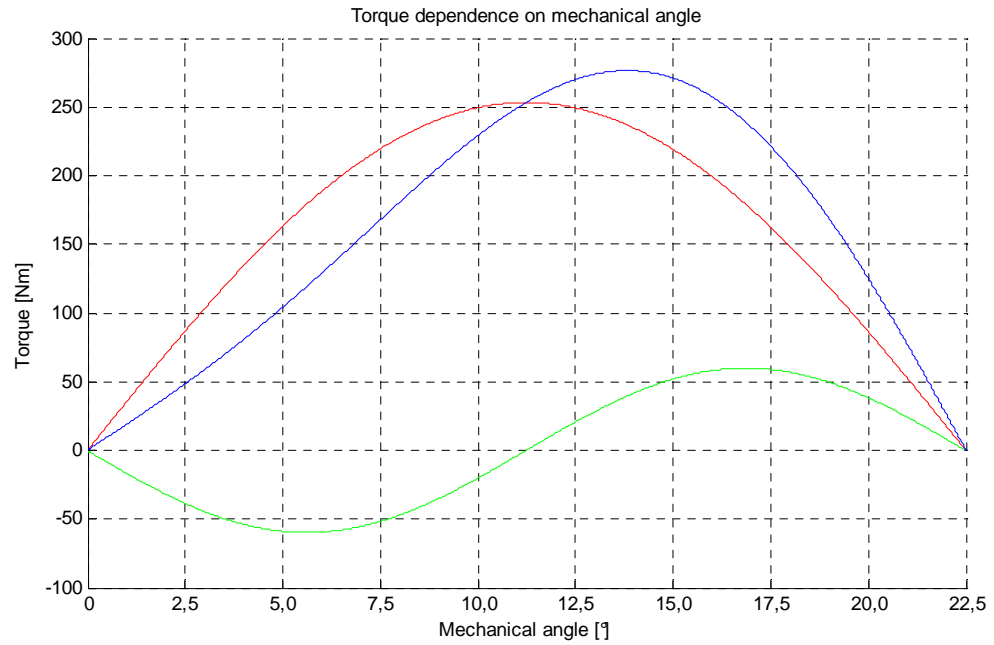

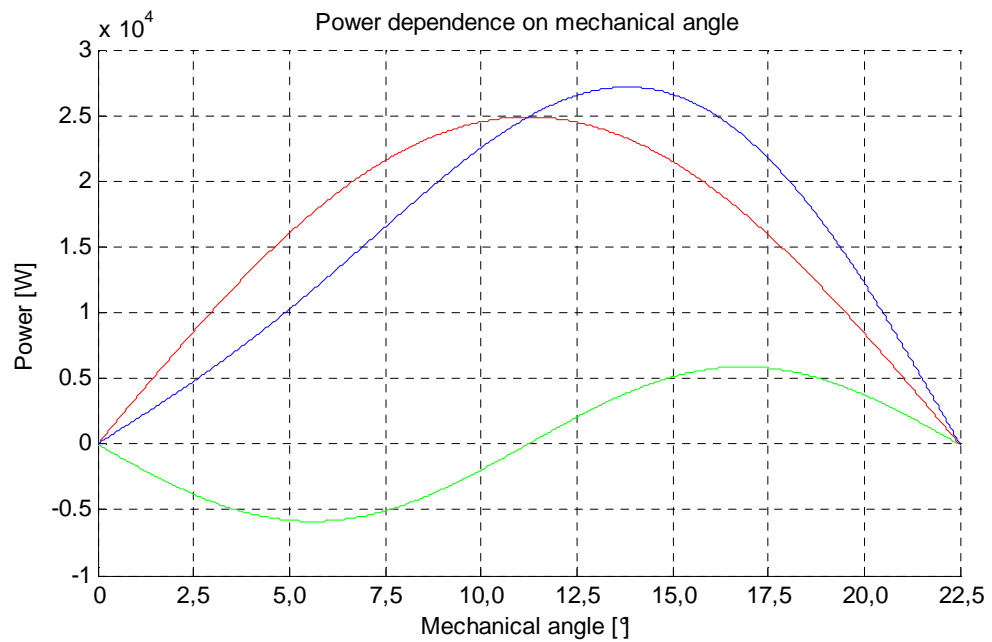Figure 4.2 Torque dependence on the mechanical load angle in a 16-pole PMSM

Figure 4.3 Power dependence on the mechanical load angle in a 16-pole PMSM

4.1.2 Torque Requirements in Passenger Vehicles

The greatest impact torque has in a passenger vehicle is observed in vehicle's acceleration. The amount of torque available is directly related to the time it takes for a vehicle of certain mass to accelerate at given acceleration. In equation (19) the relationship between force, mass and acceleration is examined.

$$F = m \cdot a \tag{20}$$

Rearranging equation (20) and rewriting force F as a function of torque and radius of the tire $F = {}^{T}\!/_{r}$ yields

$$a = \frac{T}{m \cdot r}. \tag{21}$$

In equations (20) and (21) a is acceleration and r is the radius of the tire.

Considering ERA, whose mass is 1800 kg and the radius of its tires is 0.35 m, would require total torque of 3136 Nm to accelerate at rate of 5.6 m/s^2, which is the acceleration required to propel the vehicle from 0 to 100 km/h in five seconds. Divided between four motors and not taking into account losses in the power transmission (which in ERA are negligible anyway) a total torque of 882 Nm per motor is required.

In vehicles that do not have a motor per wheel, additional mechanical losses in the mechanical power train affect the total efficiency of the vehicle. Mechanical power transmission efficiency can be assumed to be around 90 % for typical single motor configurations and slightly higher for typical two motor (motor per axle) configurations.

5. CONCLUSIONS

As stated in the Chapter 2, the continued development of related technologies and infrastructure is vital to the emergence of electric vehicle as a new standard for transportation of people and goods. While relatively complete product on an ideal level, current high cost of batteries and their limited capacity are one of the main factors holding back the electric vehicle.

When choosing components and during the design process of the electric power train and propulsion system, attention must be paid to ensure that the system will fulfill the requirements set for EMC and to ensure safe operation at all times. Effects of EMI can be reduced by shielding all the components and systems prone to cause or suffer from EMI. Also ferrite rings can be used around conductors to limit the common and differential mode currents.

There are several types of electric motors and several different ways to use them in an electric vehicle. The optimal configuration depends on the type of the vehicle and desired properties: Desired power, acceleration, energy efficiency, total weight and cost. Induction motors offer high power with low cost, but suffer from low starting torque and lower efficiency when compared to synchronous motors. Synchronous motors have high power and high starting torque but are more expensive and have reduced lifetime when compared to induction machines and depending on the type of the synchronous motor, may have difficulties when operating in field weakening region.
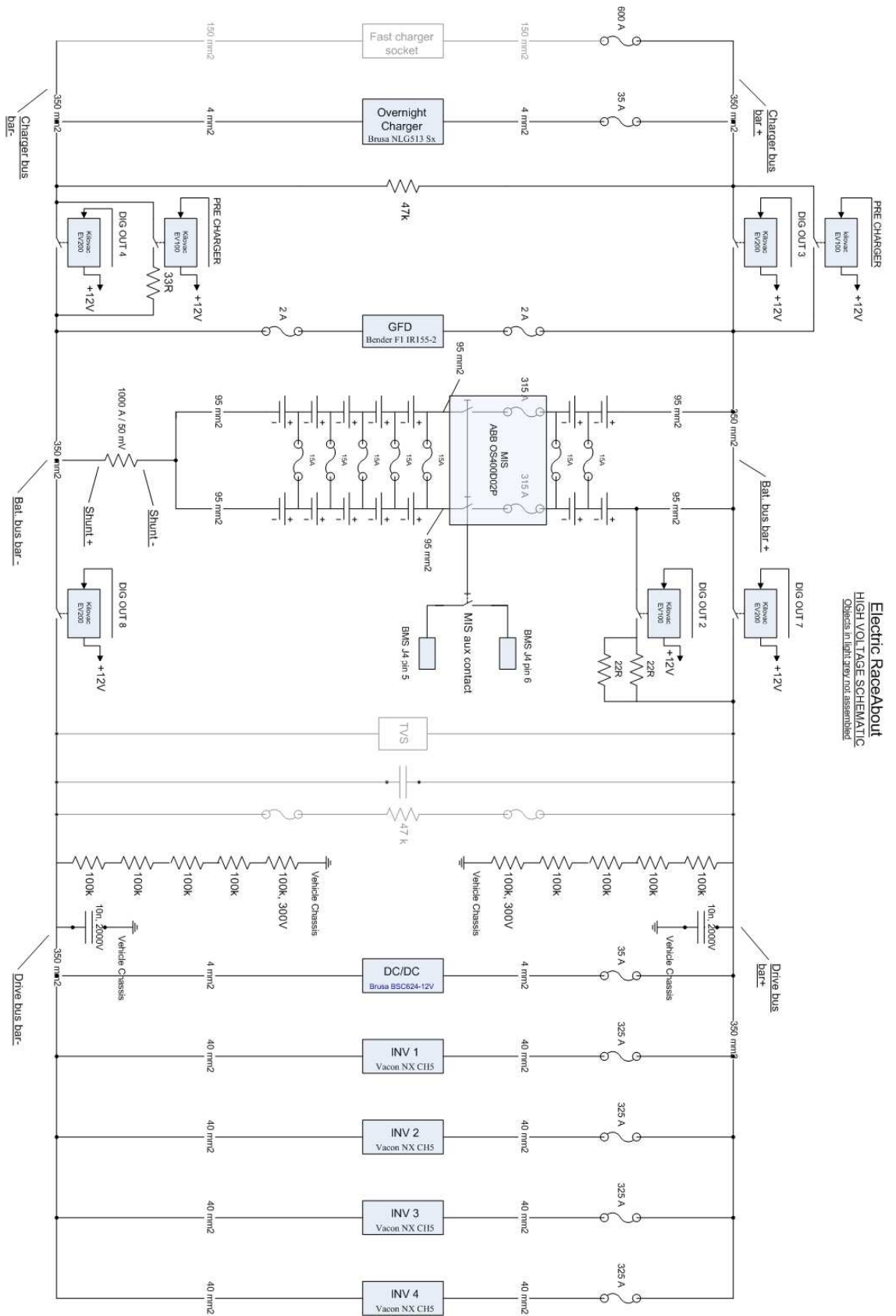
REFERENCES

/1/ *Energy Statistics Yearbook 2008* [statistic data] [referred 22.01.2010] Available: www.tilastokeskus.fi/energia

/2/ *Tuontiauton ajomäärä verotuksessa* [web article] [referred 02.02.2010] Available: http://www.autovero.fi/artikkeli.php?aid=26

/3/ Energiateollisuus ry. *Production and Foreing Trade of Electricity* [web article] [referred 20.9.2009]. Available: http://www.energia.fi/fi/tilastot/sahkotilasto/tuotanto/sahkontuotantotuontijavienti

/4/ Parliamentary Office of Science and Technology. *Carbon Footprint of Electricity Generation* [web document] [referred 22.09.2009]. Available: http://www.parliament.uk/documents/upload/postpn268.pdf

/5/ *Regulation (EC) No 443/2009 of the European Parliament and of the Council of 23 April 2009 setting emission performance standards for new passenger cars as part of the Community's integrated approach to reduce CO 2 emissions from light-duty vehicles Text with EEA relevance* [web document] [referred 27.03.2010] Available: http://eur-lex.europa.eu/LexUriServ/LexUriServ.do?uri=OJ:L:2009:140:0001:01:EN:HTML

/6/ Mitsubishi Motors Corporation; Kazunori, H., Hiroaki, Y. *Development of Next-Generation Electric Vehicle "i-MiEV"* [research report] [referred 20.02.2010] Available: www.mitsubishi-motors.com/corporate/about_us/technology/review/e/pdf/ 2007/19e_12.pdf

/7/ Altairnano. *50Ah Lithium titanate battery cell* [datasheet] [referred 26.10.2009]. Available: http://www.b2i.cc/Document/546/50Ah_Datasheet-012209.pdf

/8/ Mohan, Undeland et Robbins. *Power Electronics - Third Edition* [ISBN: 978-0-471-22693-2]

/9/   Brusa. *NLG523-Wx Manual* [Manual] [referred 6.4.2010] Available: http://www.brusa.biz/e_manuals.htm

/10/   Brusa. *BSC624-12V Manual* [Manual] [referred 7.4.2010] Available: http://www.brusa.biz/e_manuals.htm

/11/   A-*ISOMETER® iso-F1 (IR155-1 / IR155-2* [datasheet] [referred 02.03.2010] Available: http://www.iso-f1.com/downloads.html

/12/   *Kilovac EV200* [datasheet] [referred 02.03.2010] Available: http://www.kilovac.com/kilovac/

/13/   Silventoinen, P. *Electromagnetic compatibility and EMC-measurements in DC-voltage link converters,* Acta Universitatis Lappeenrantaesis 112,   dissertation [ISBN: 951-764-588-0]

/14/   Kuisma, M. *Minimizing conducted RF-emissions in switch mode power supplies using spread-spectrum techniques*, Acta Universitatis Lappeenrantaesis 177, dissertation [ISBN: 951-764-874-X]

/15/   Skibinski, G., Kerkman, R. et Schlegel, D. *EMI emissions of modern PWM AC drives,* IEEE Industry Applications Magazine, vol.5, Issue 6, pp. 47-81.

/16/   Ström, J-P. *Active du/dt filtering for variable-speed AC drives*, Acta   Universitatis Lappeenrantaesis 378, dissertation [ISBN: 978-952-214-888-9]

/17/   *SKINTOP® MS-SC-M Datasheet* [datasheet] [referred 10.04.2010] Available: http://www.lappgroup.com/

/18/   Vacon. *User Manual For NX-series Liquid Cooled Converters* [manual] [referred 01.05.2010] Available: http://www.vacon.fi/

/19/   *ERA PMSM Technical Specification* [technical specification] [referred 11.04.2010]

/20/   Oak Ridge National Laboratory. *REPORT ON TOYOTA/PRIUS MOTOR DESIGN AND MANUFACTURING ASSESSMENT* [report] [referred 01.05.2010]
Available: http://www.ornl.gov/~webworks/cppr/y2001/rpt/120761.pdf

/21/   Pyrhönen, J. *Electric Machines Lecture Material* LUT 2006

/22/   Pyrhönen, J. *Design Of An Electric Machine Lecture Material* LUT 2006

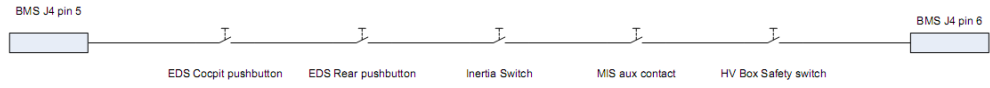# APPENDIX I-1

Electric Propulsion System Schematic

APPENDIX I-2

Relay control signal path

BMS J4 pin 5

BMS J4 pin 6

EDS Cocpit pushbutton   EDS Rear pushbutton   Inertia Switch   MIS aux contact   HV Box Safety switch

APPENDIX II - Matlab scripts

Battery efficiency

```
%Calculating battery pack losses

I=[0:1:1000];                    %Current vector
Rpack=(143*28*10^-4)/2;          %Battery pack resistance
Ploss=I.^2*Rpack;                %I^2*R losses
Ubatt=[372:-0.036:336];          %Battery voltage linearization
Pout=Ubatt.*I;                   %Battery output power

figure()
hold on
axis([0 1000 0 350000])
xlabel('Current [A]');
ylabel('Losses [W]');
title('Losses caused by the internal resistance in the battery pack')
plot(Ploss,'r');plot(Pout,'b');  %Battery output and losses, plotting

figure();
hold on;grid on
axis([0 1000 0 210])
xlabel('Current [A]');
ylabel('Internal voltage drop [U]');
title('Internal battery voltage drop');
Ubattloss=I.*Rpack;
plot(Ubattloss);                 %Battery voltage drop
```

Drag and air resistance

```
%Calculating drag and rolling friction

v=[0:1:56];              %Car velocity vector
Aera=2;                  %Resisting area
Cd=0.25;                 %Form coefficient
p=1.2;                   %Air density
mass=1600;               %Vehicle mass

Fdrag=0.5*p*v.^2*Cd*Aera;        %Calculating drag
Ffric=mass*9.81*0.0105+v.*0;     %Calculating rolling friction
Ftot=Fdrag+Ffric;                %Calculating total resistance

figure()
hold on
axis([0 56 0 1200])
xlabel('Velocity [km/h]');
ylabel('Drag [N]');
title('Drag dependance on vehicle velocity')
plot(Fdrag,'r');plot(Ffric,'g');plot(Ftot,'b'); %Plotting the results
```